Lecture 14: NMR Spectroscopy of Glass – Practice and Application : Quadrupolar Nuclei

- Examine alkali borate glasses and the formation of tetrahedral borons
- Examine alkali thioborate glasses and the formation of tetrahedral borons
- Examine temperature dependence of spin lattice relaxation rate to probe ion dynamics in glass

I = 3/2 ^{11}B, ^{27}Al….

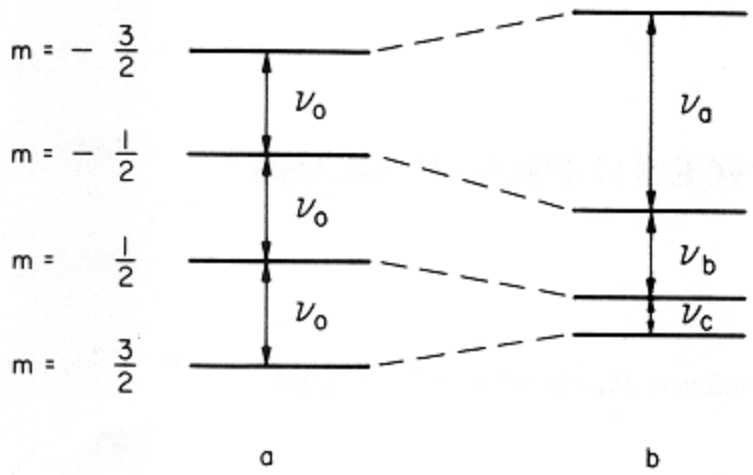

Fig. 1. Energy levels arising from the interaction of the nuclear magnetic moment with a magnetic field: (a) unperturbed Zeeman interaction; (b) perturbation interaction present. The levels shown are appropriate for a nucleus such as ^{11}B with spin $I = \frac{3}{2}$.

Bray JNCS 73(1985)19-45

Powder pattern, amorphous, lineshape for I = 3/2

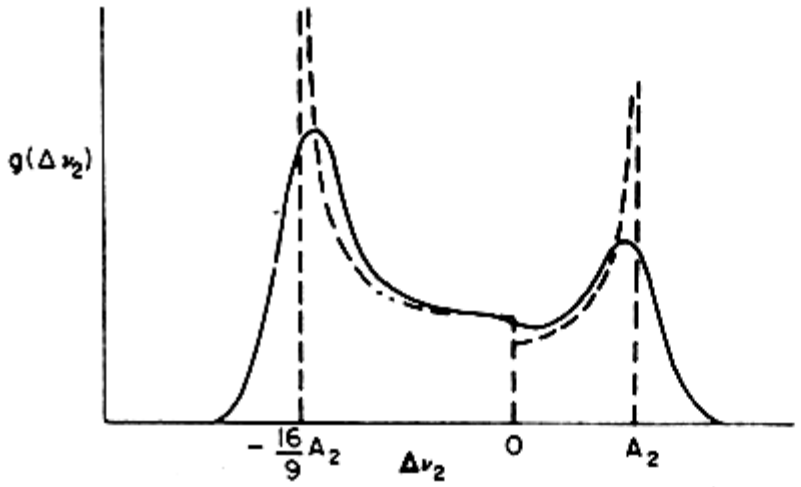

Fig. 2. Second-order quadrupole broadened powder pattern for the central transition of a half-integer spin. Dashed line: no dipolar broadening present. Solid line: dipolar broadening present.

Bray JNCS 73(1985)19-45

^{11}B NMR lineshapes for v=B_2O_3

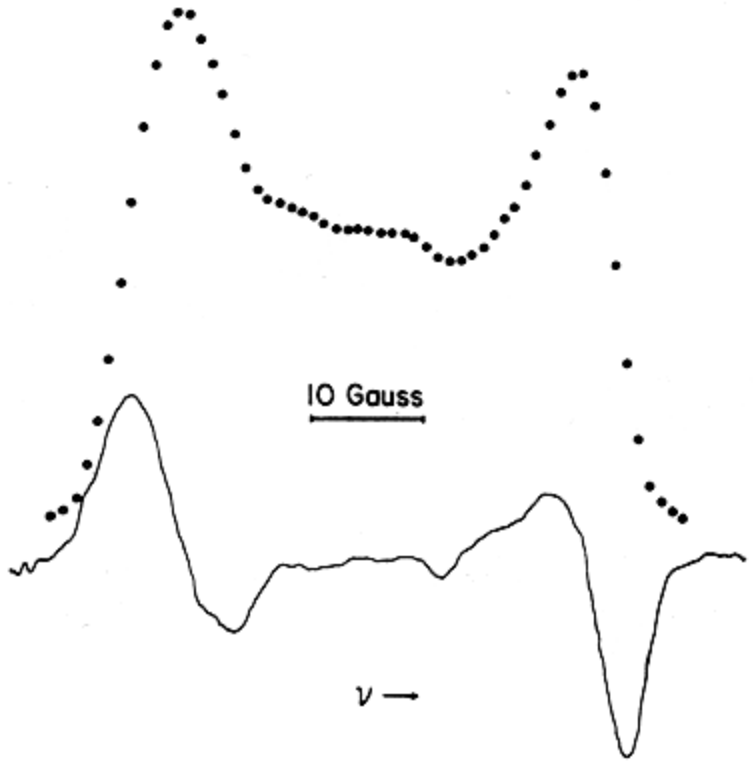

Fig. 3. The solid curve is the experimental derivative spectrum, absorption mode, of ^{11}B in vitreous B_2O_3. Open circles represent the absorption obtained by numerical integration of the experimental curve.

Bray JNCS 73(1985)19-45

Theoretical line shapes for I = 3/2 spin

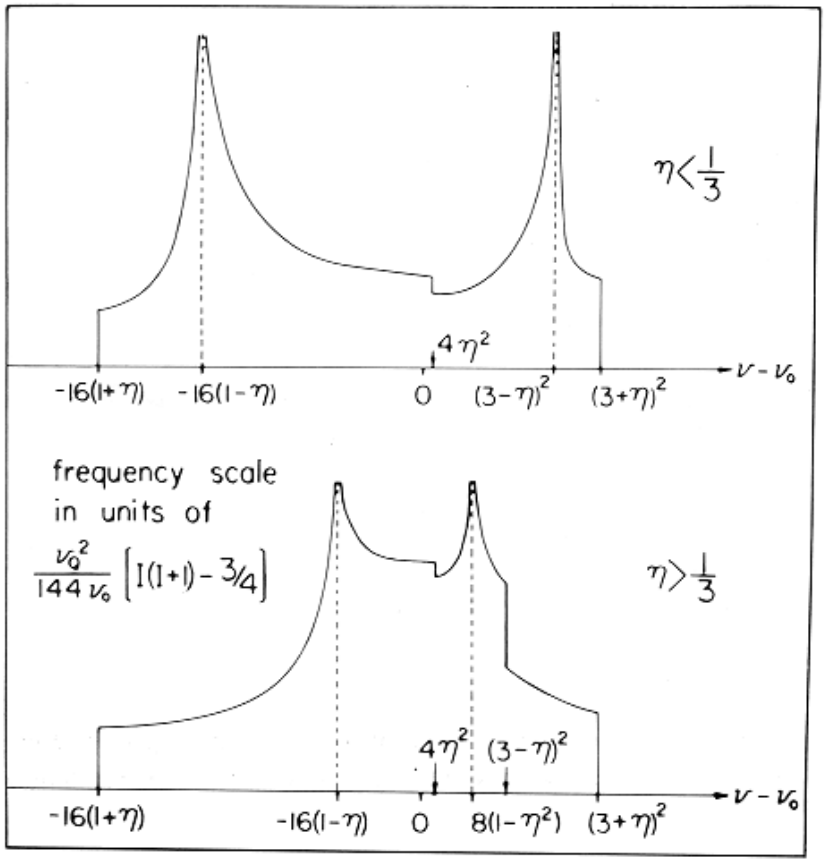

Fig. 4. Powder patterns for the central transition ($m = -\frac{1}{2} \leftrightarrow \frac{1}{2}$) of half-integer nuclei in the presence of second-order quadrupole interactions for two regimes: $\eta < \frac{1}{3}$ and $\eta > \frac{1}{3}$.

Bray JNCS 73(1985)19-45

NMR "wide line" CW spectra of v-B_2O_3

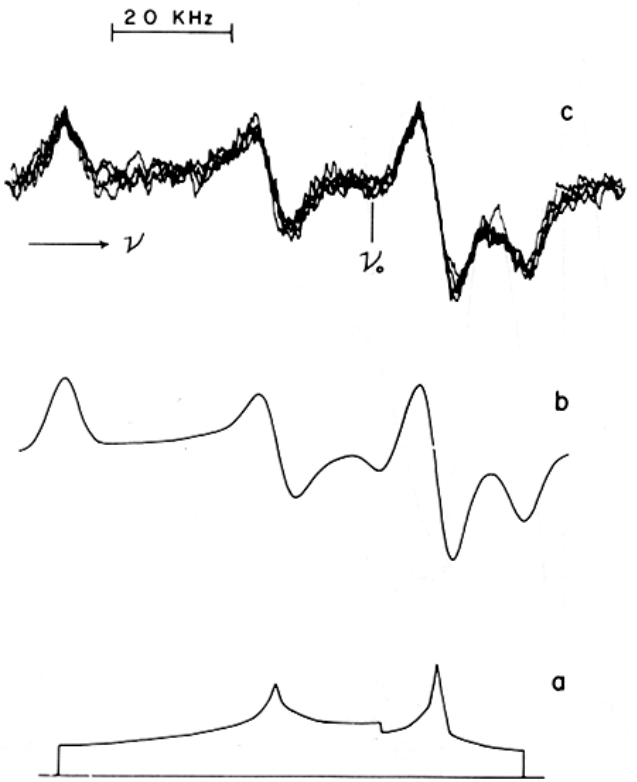

Fig. 5. (a) Theoretical powder pattern for the transition ($m = \frac{1}{2} \leftrightarrow m = -\frac{1}{2}$), with $I = \frac{3}{2}$, $\nu_0 = 16$ MHz, $e^2qQ/h = 2.56$ MHz, and $\eta = 0.54$. (b) First derivative of the theoretical pwder pattern after convolution with a gaussian curve of linewidth $2\sigma = 5$ kHz. (c) Superposition of four experimental traces for ^{11}B in polycrystalline calcium metaborate, at a resonant frequency of 16 MHz.

Bray JNCS 73(1985)19-45

Computer simulation of ^{11}B NMR CW static spectra

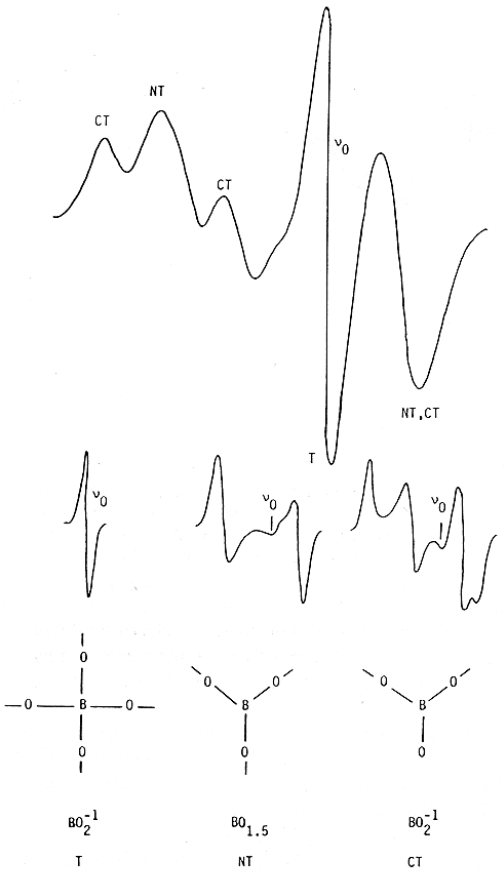

Fig. 6. The upper portion of this figure shows a computer simulation of a typical ^{11}B NMR derivative spectrum in a borate glass having high alkali oxide content. The spectrum is a superposition of three responses labelled T, NT, and CT shown in the middle portion of the figure. The lower portion of the figure depicts the boron–oxygen configurations corresponding to the NMR responses shown above. These are the tetrahedral (T) configuration, the neutral trigonal (NT) configuration, and the charged trigonal (CT) configuration.

Bray JNCS 73(1985)19-45

Comparison of derivative and integrated spectra

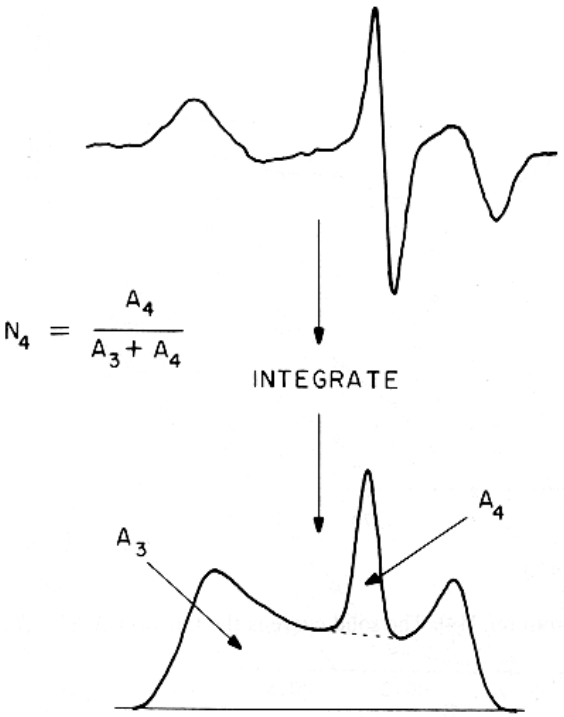

Fig. 7. The top curve is a computer simulation of a typical ^{11}B experimental spectrum obtained from alkali borate glasses near the tetraborate composition. The bottom curve is the true power absorption spectrum, which is the integral of the top curve. The areas under the absorption curve which result from the boron atoms in tetrahedral or trigonal coordination are labelled as A_4 and A_3 respectively.

Bray JNCS 73(1985)19-45

Fraction of tetrahedral borons in alkali borate glasses

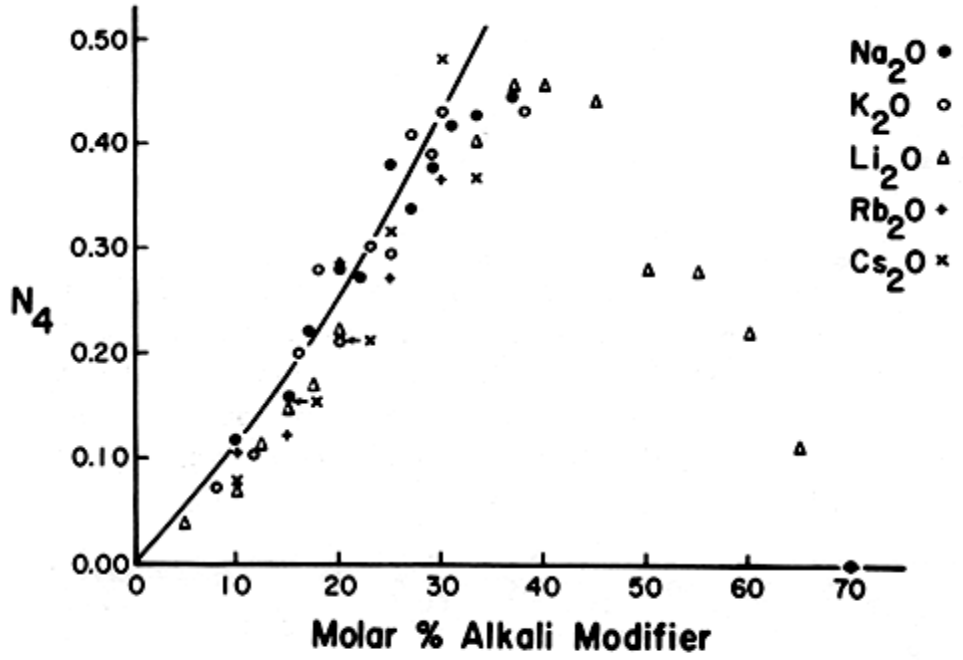

Fig. 8. The fraction N_4 of boron atoms in four coordination in alkali borate glasses. ● Na_2O, Δ Li_2O, × Cs_2O, ○ K_2O, + Rb_2O.

Bray JNCS 73(1985)19-45

Structural groups in alkali borate glasses

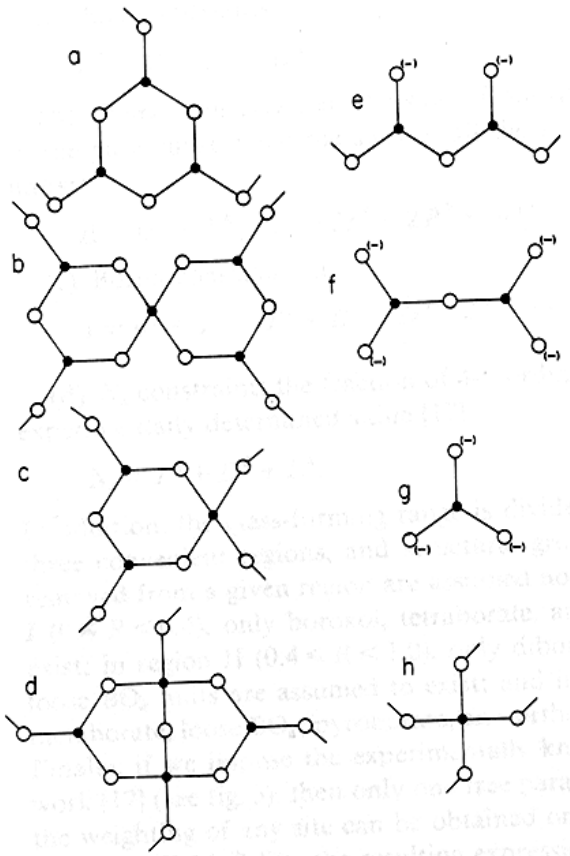

Fig. 2. Structural groupings in lithium borate glasses. Solid circles represent boron atoms, open circles oxygen atoms. An open circle with a negative sign indicates a non-bridging oxygen. (a) boroxol unit (b) pentaborate unit (c) triborate unit (d) diborate unit (e) metaborate unit (f) pyroborate unit (g) orthoborate unit (h) loose BO_4 unit. A tetraborate unit is formed by connecting one oxygen of the BO_4 unit in the triborate unit to a BO_3 unit of the pentaborate unit.

Feller, Dell, and Bray JNCS 51(1982)21-30

B_2O_3 glass

- B_2O_3 glass exhibits high level of IRO
- Triangles form 6 membered "boroxyl" rings
- 25% of borons are not in rings
  - $BO_{3/2}$ "loose" triangles
- 75% of borons are in rings
  - $B_3(O)_3(O_{3/2})$
- Equal numbers of boroxyl rings and loose triangles

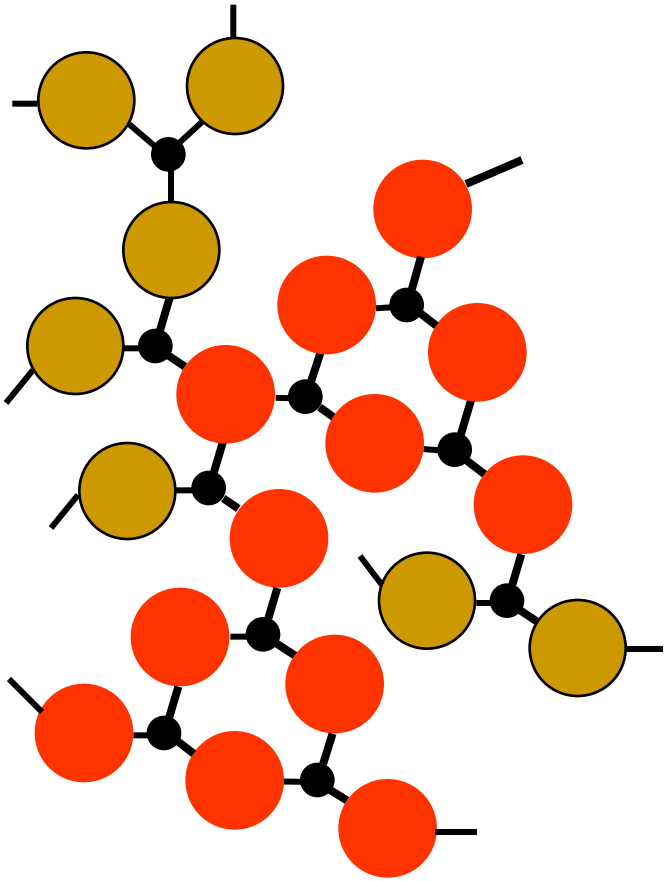

Tetrahedral boron formation in alkali borate glasses

- $M^{+}BO_{4/2}^{-1}$ units form with the addition of M_2O to $BO_{3/2}$
- Two tetrahedral units form, for every M_2O added
- $xM_2O + (1-x)B_2O_3$ >>
  $f(BO_{4/2}) \equiv N_4 = [BO_4]/\text{Total B}$
  $= 2x/2(1-x)$
  $= x/(1-x)$
- B fills it's shell with octet of electrons
- Alkali ion acts as a "spectator"ion not actively involved in bonding

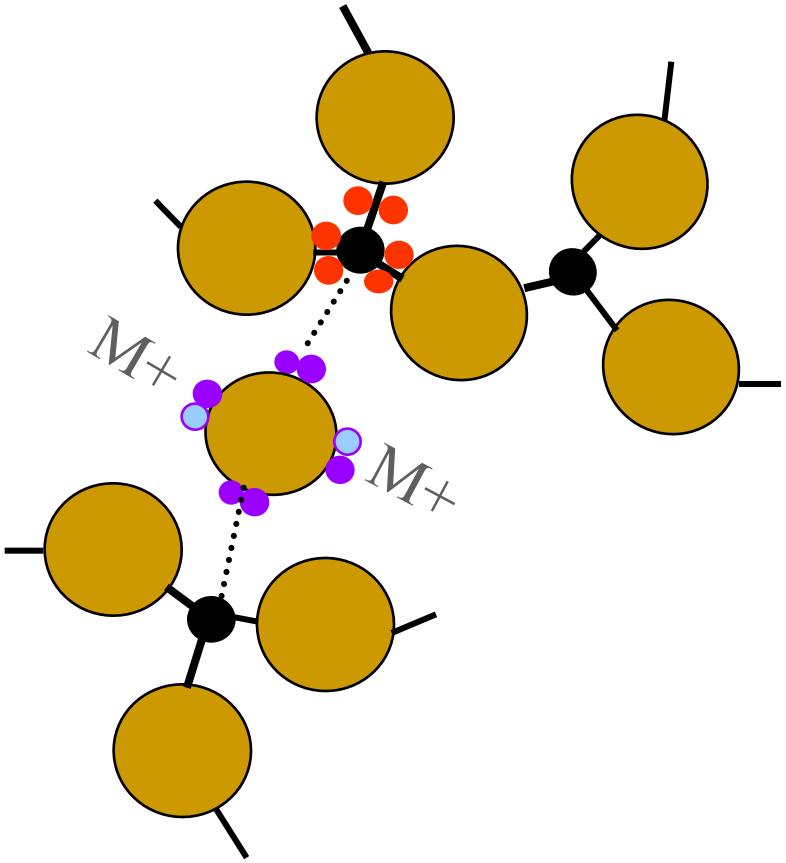

Alkali modified borate glasses

- $M_2O + B_2O_3$ glasses
- $BO_{3/2}$ has 6 valence electrons
- Three B-O single bonds
- B can lower it's energy by forming four B-O single bonds to over to 8 (full "octet") valence electrons
- It can do so by using M_2O ($M_2^{2+}O^{=}$) an electron donor
- $xM_2O + (1-x)B_2O_3$ >>

  $f(BO_{4/2}) \equiv N_4 = [BO_4]/\text{Total B}$

  $= 2x/2(1-x)$

  $= x/(1-x)$

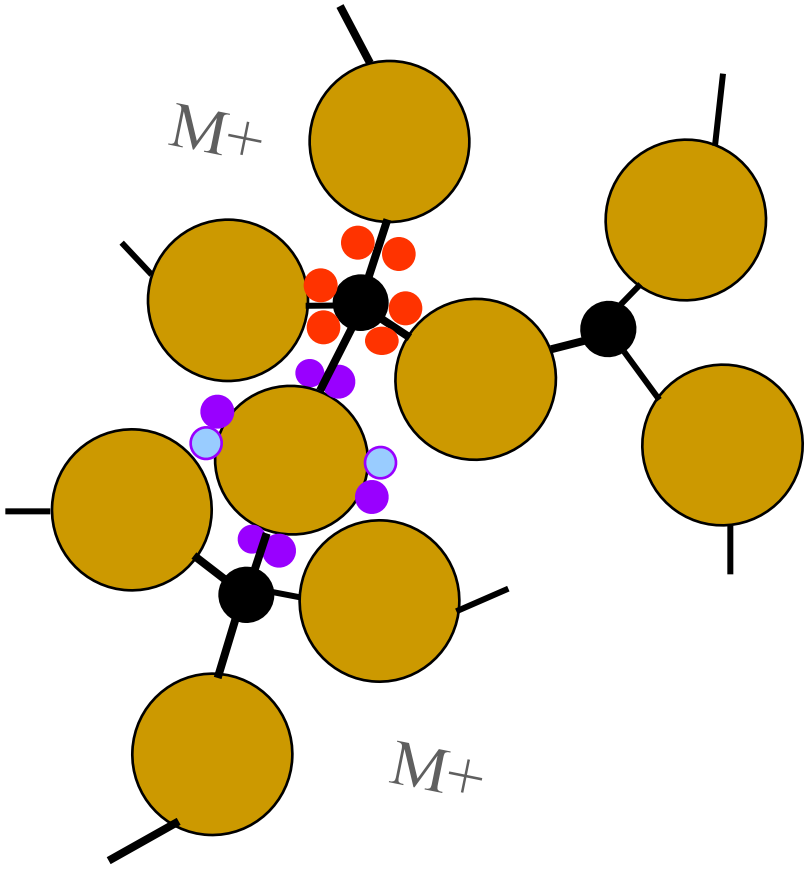

Tetrahedral boron formation in alkali borate glasses

- Two tetrahedral borons form for every M^+ added
- Alkali ions are “spectator” ions in the reaction
- All of the alkali ions, Li, Na, K, Cs, and Rb act in the same manner
- Affect is for M_2O to cross-link borate glass structure
- $xM_2O + (1\text{-}x)B_2O_3$ >>

  $f\ (BO_{4/2}) \equiv N_4 = [BO_4]/\text{Total B}$

  $= 2x/2(1\text{-}x)$

  $= x/(1\text{-}x)$

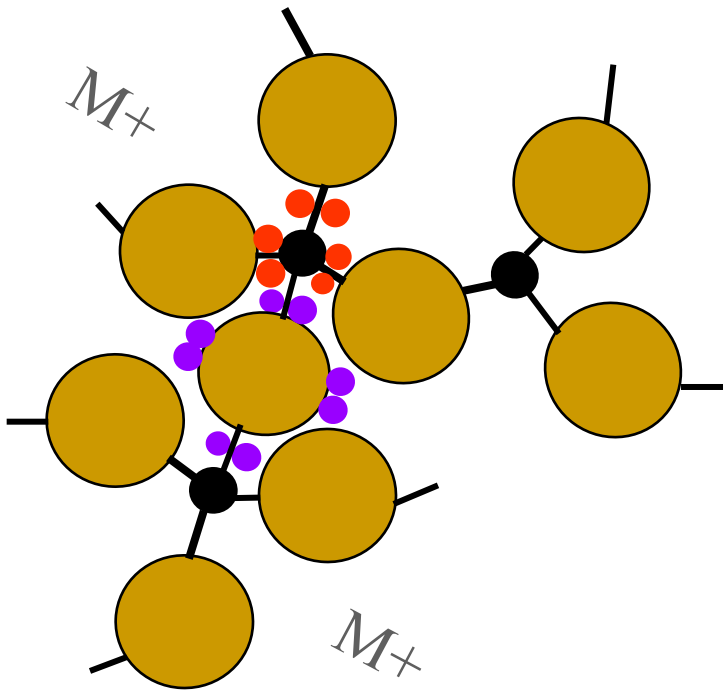

Structure and NMR characteristics of various borate groups

Table 1.
Structural groupings in the lithium borate system and associated quadrupole parameters used in this study. The chemical formulas are chosen to correspond to fig. 2.

Structural grouping	Chemical formula	Composition (R)	Fraction label	Q_{cc} (MH_z)	η	$\sigma_{Q_{cc}}$ (MH_z)	σ_η
Boroxol	$\frac{1}{3}(B_2O_3)$	0.0	B^3	5.45	0.12	0.22	0.05
Tetraborate	$Li_2O\cdot 4B_2O_3$	0.25	T^3	5.45	0.26	0.22	0.05
	$=2(Li^{1+})+(B_8O_{13})^{2-}$		T^4	0.6	0.5	0.2	0.5
Diborate	$Li_2O\cdot 2B_2O_3$	0.5	D^3	5.45	0.08	0.22	0.05
	$=2(Li^{1+})+(B_4O_7)^{2-}$		D^4	1.1	0.5	0.5	0.5
Loose BO_4	$Li_2O\cdot B_2O_3$	1.0	L^4	1.1	0.5	0.5	0.5
	$=2[(Li^{1+})+(BO_2)^{1-}]$						
Metaborate	$Li_2O\cdot B_2O_3$	1.0	M^3	5.45	0.55	0.22	0.05
	$=2(Li^{1+})+(B_2O_4)^{2-}$						
Pyroborate	$2Li_2O\cdot B_2O_3$	2.0	P^3	5.45	0.55	0.22	0.05
	$=4(Li^{1+})+(B_2O_5)^{4-}$						
Orthoborate	$3Li_2O\cdot B_2O_3$	3.0	O^3	5.75	0.0	0.22	0.05
	$=2[3(Li^{1+})+(BO_3)^{3-}]$						

Feller, Dell, and Bray JNCS 51(1982)21-30

Composition dependence of structural groups in $Li_2O + B_2O_3$ glasses

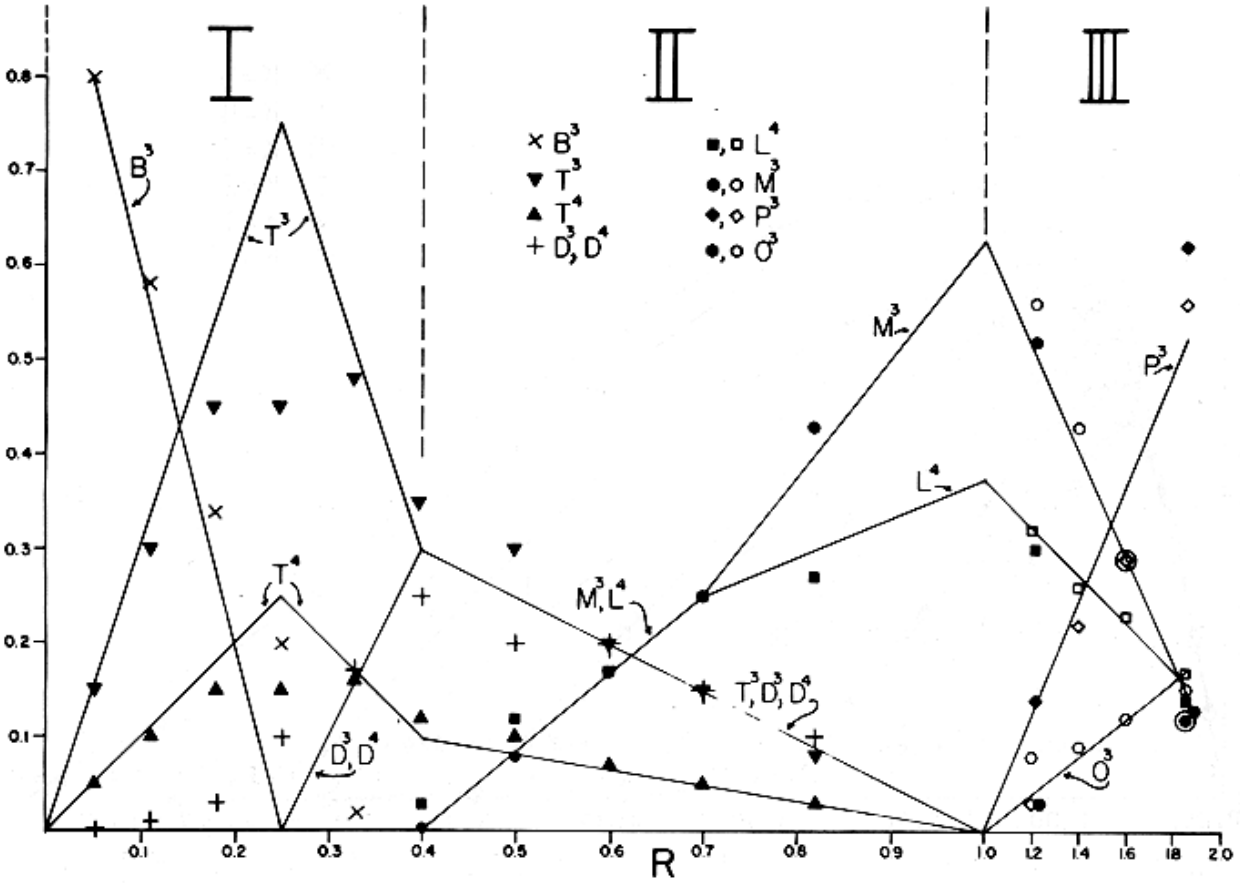

Fig. 13. The relative amounts of each type of structural grouping present in lithium borate glasses as a function of R = mol.% Li_2O/mol.%B_2O_3. See text for definitions of symbols.

Feller, Dell, and Bray JNCS 51(1982)21-30

B MASS NMR of alkali borate glasses

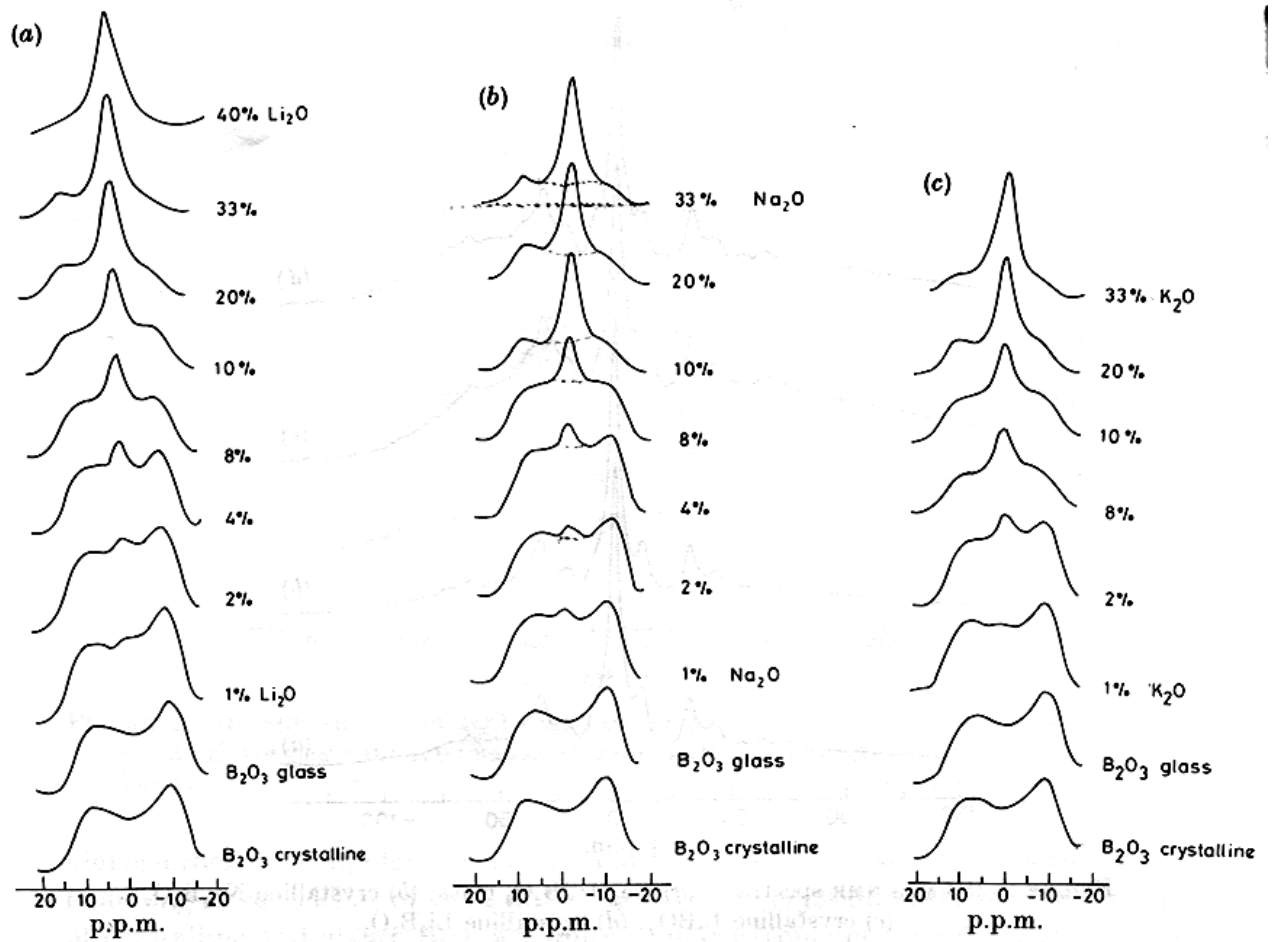

FIGURE 4. ^{11}B MAS NMR resonance lineshapes of (*a*) $Li_2O \cdot B_2O_3$, (*b*) $Na_2O \cdot B_2O_3$ and (*c*) $K_2O \cdot B_2O_3$ glasses.

Prabakar, Rao, and Rao, Proc. R. Soc. Lond. A 429(1990)1-15

High field high spin rate B MASS NMR

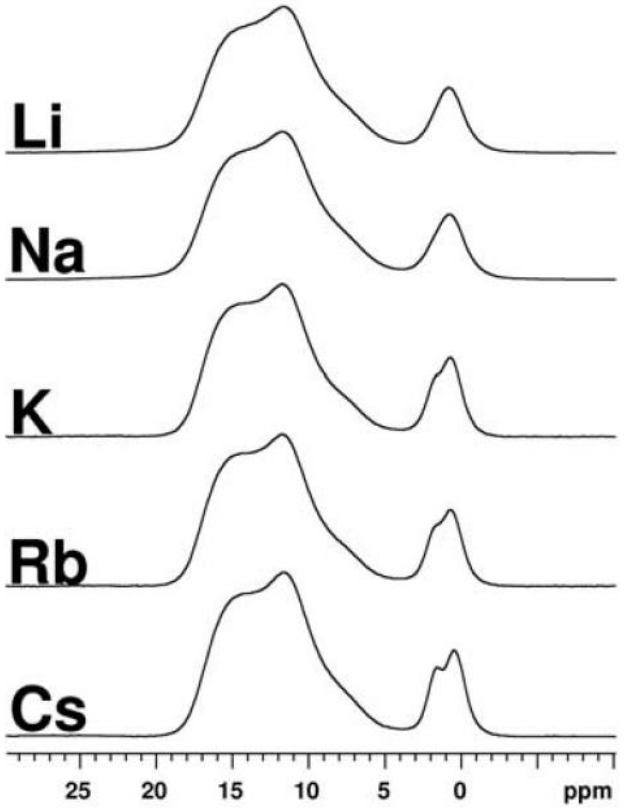

Figure 1. ^{11}B MAS NMR spectra of alkali borate glasses (R=0·1) collected at 14·1 T with spinning speeds of 16 kHz

Proc. Fifth Int. Conf. on Borate Glasses, Crystals and Melts *Phys. Chem. Glasses: Eur. J. Glass Sci. Technol. B*, August 2006, 47 (4), 393–396

Fraction of B4 in alkali borate glasses

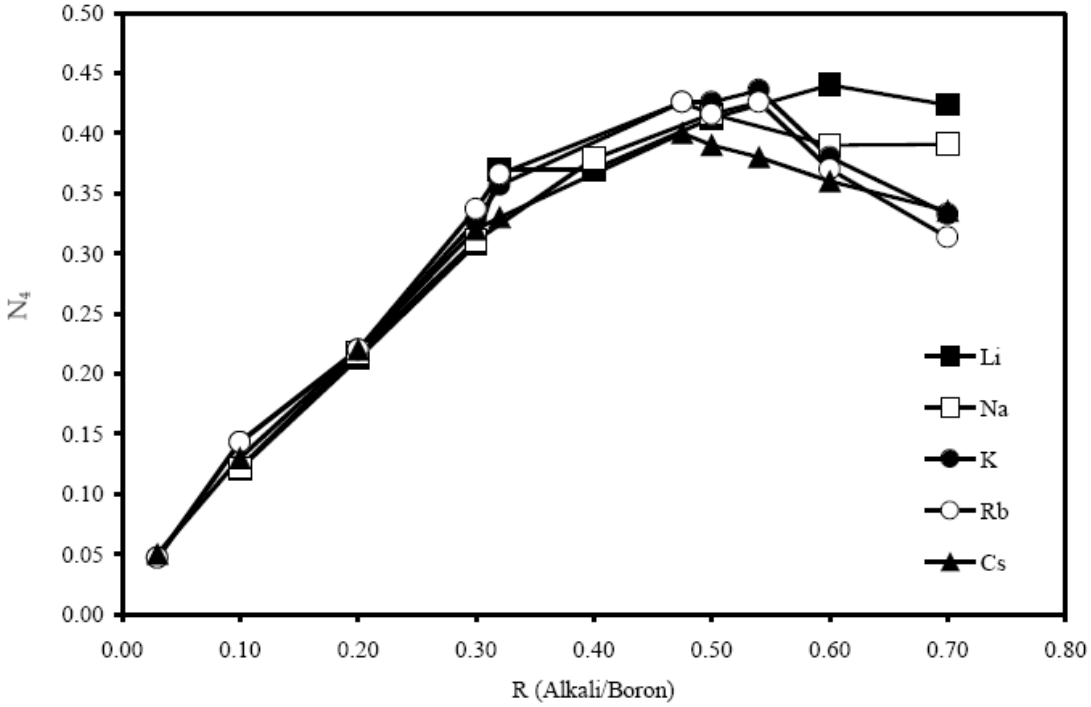

Figure 2. Four-coordinate boron fraction as a function of composition, for alkali borates

Proc. Fifth Int. Conf. on Borate Glasses, Crystals and Melts *Phys. Chem. Glasses: Eur. J. Glass Sci. Technol. B*, August 2006, 47 (4), 393–396

B4 in alkali borosilicate glasses

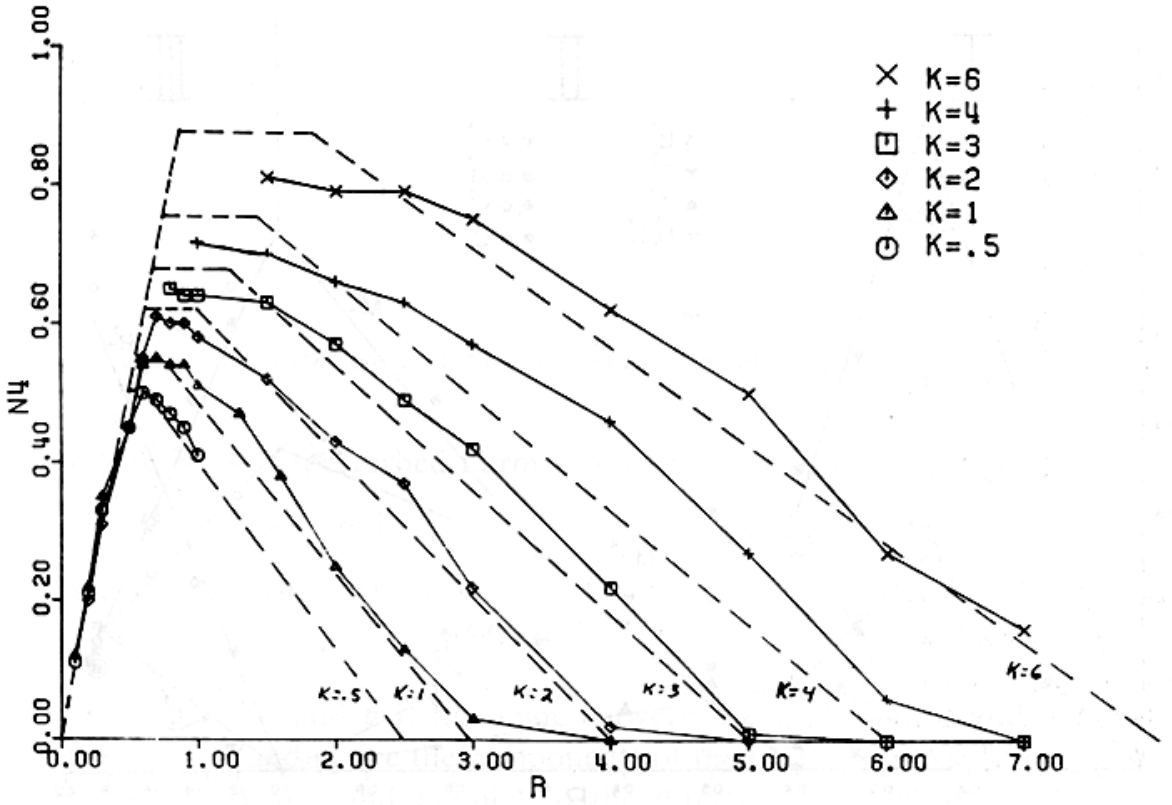

Fig. 11. Composite of N_4 data for glasses in the system $Na_2O–B_2O_3–SiO_2$. The dashed lines are predictions based on the model presented in ref. [18].

Bray JNCS 73(1985)19-45

B3 in alkali borate glasses

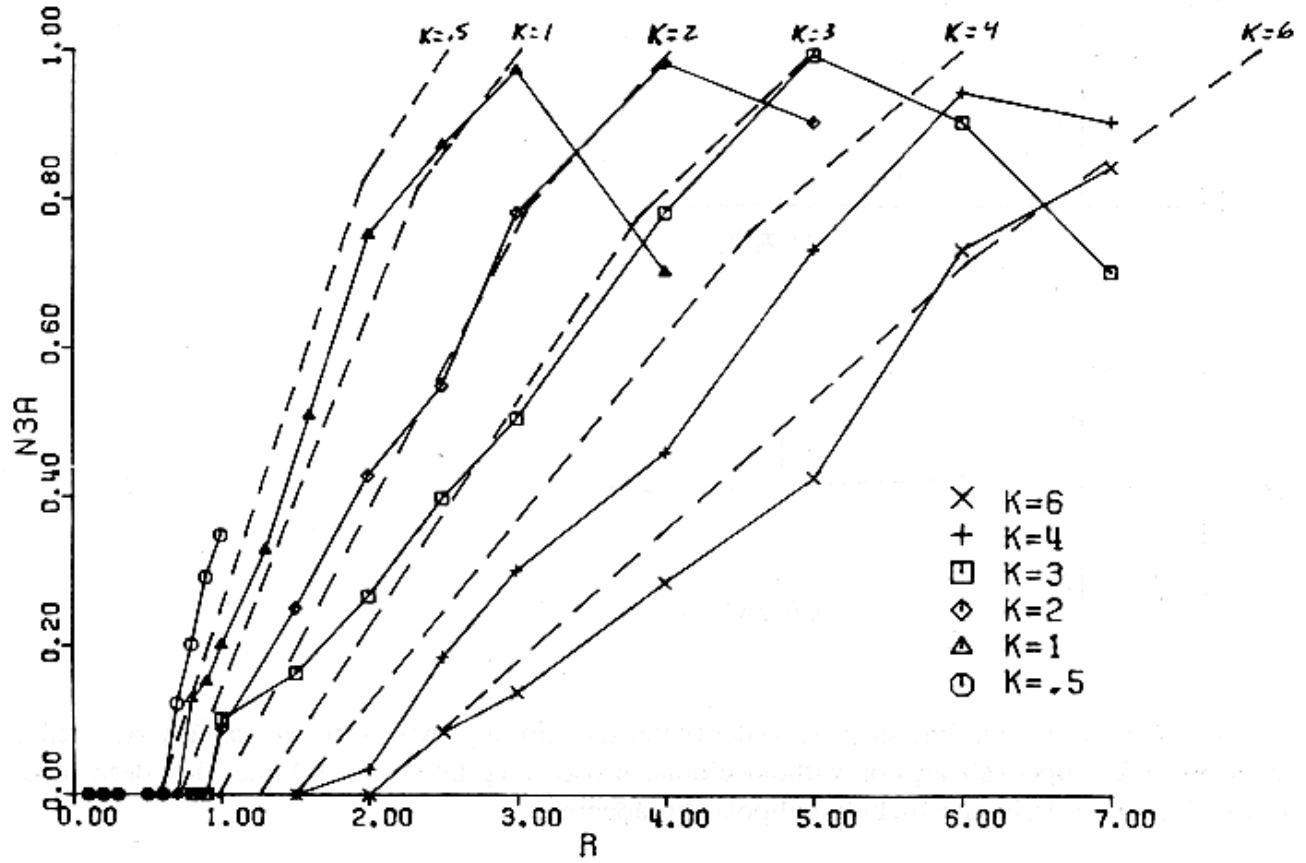

Fig. 12. Composite of N_{3A} data for glasses in the system Na_2O–B_2O_3–SiO_2. The dashed lines are predictions based on the model presented in ref. [18].

Bray JNCS 73(1985)19-45

2D MASS NMR of ^{11}B in B_2O_3

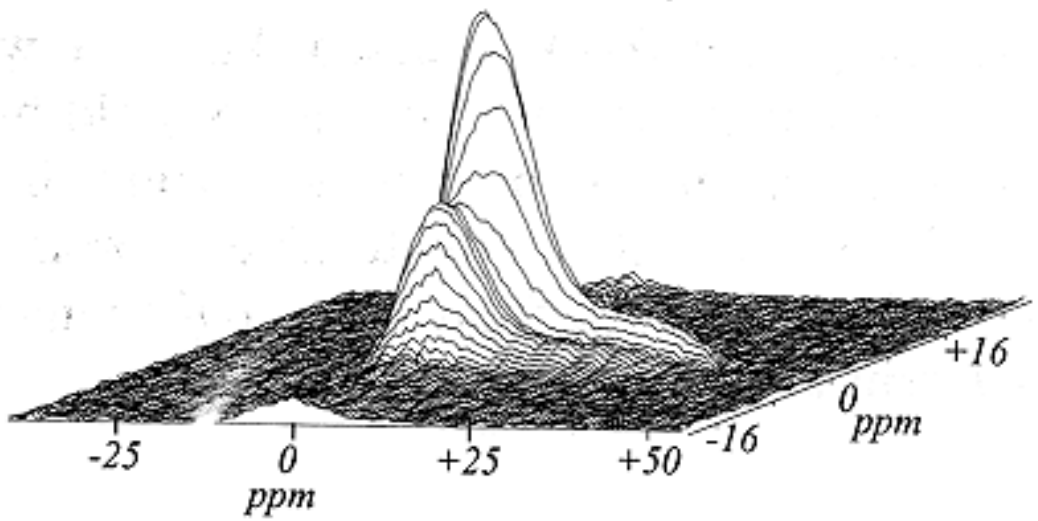

Fig. 1. The 2D DAS-NMR spectrum of ^{11}B in glassy B_2O_3, enriched to 97% ^{10}B, at 8.4 T (115.6 MHz). The shift is reported relative to $Et_2O \cdot BF_3$. The chemical shift axes are reversed from the normal NMR convention in order to show better the less intense spectral component.

Zwanziger, Youngman JNCS 168(1994)293-297

2D ^{11}B MASS NMR

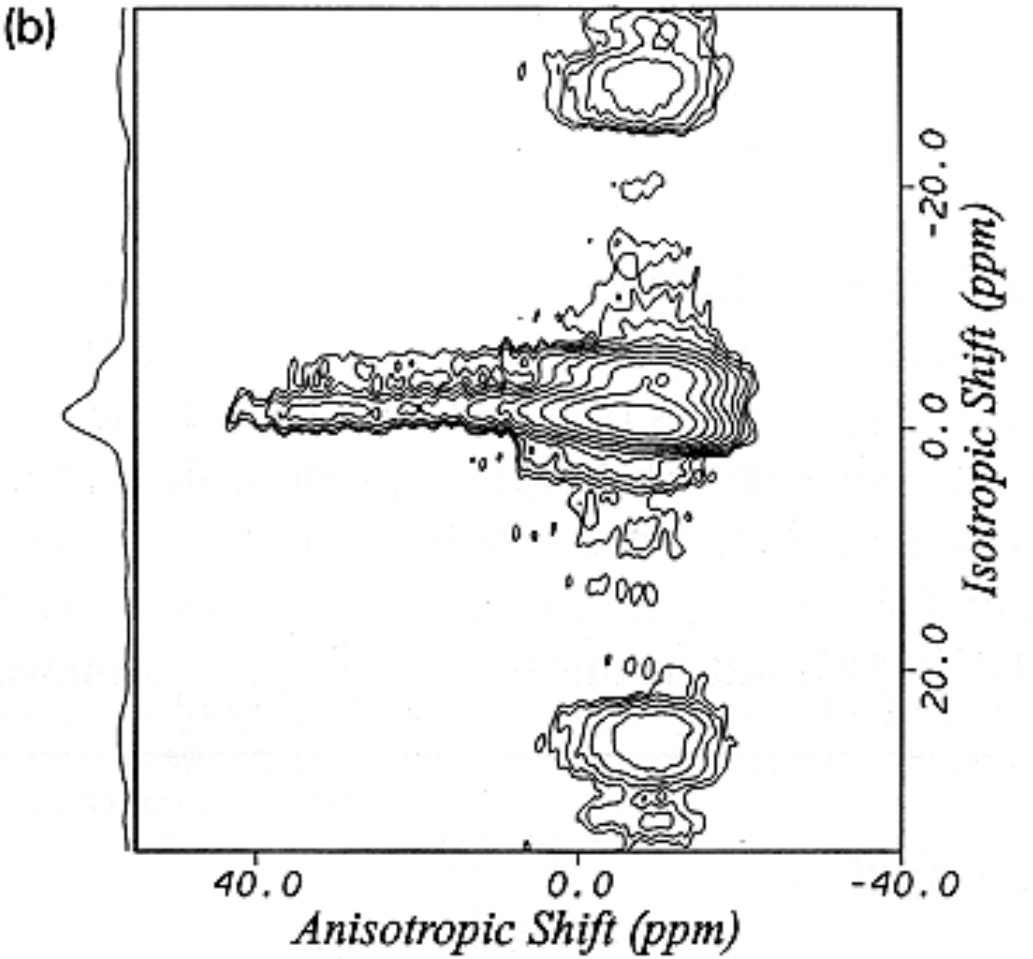

Zwanziger, Youngman JNCS 168(1994)293-297

2D ^{11}B MASS NMR

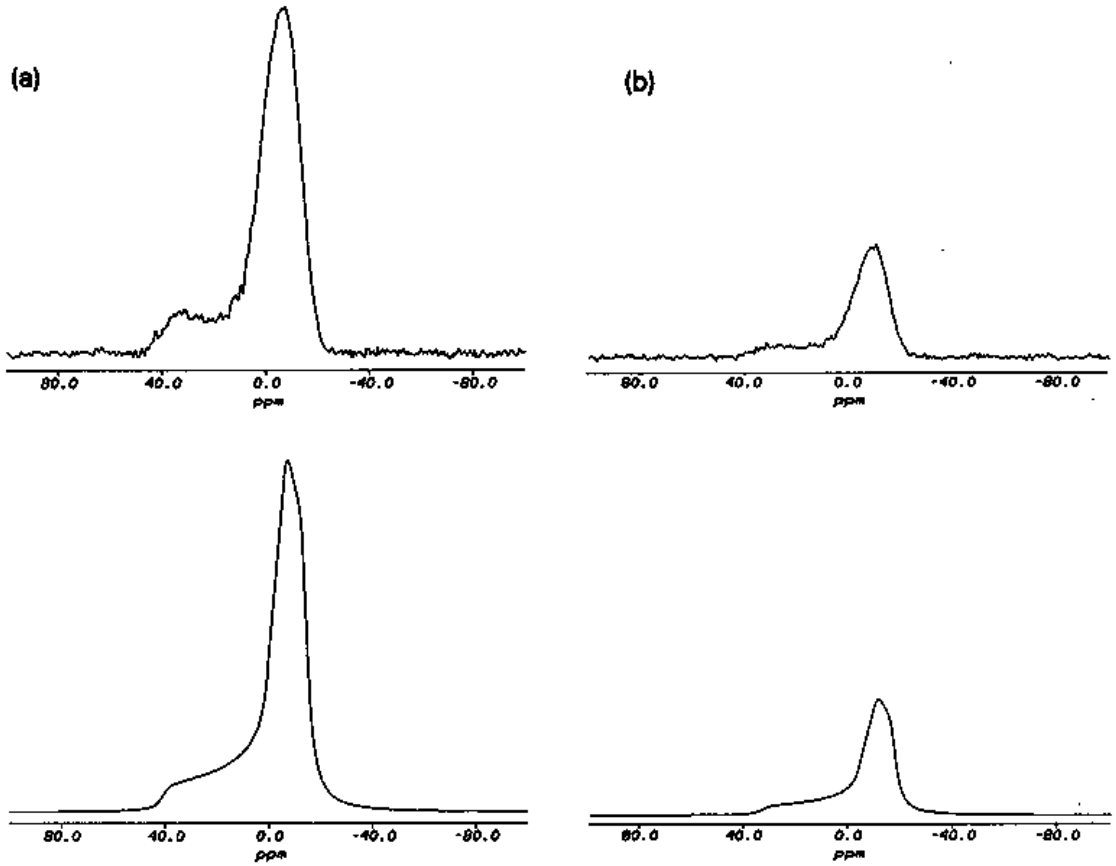

Fig. 3. The anisotropic powder patterns for the two boron sites, extracted from the 2D data set at 7.1 T by taking slices at the isotropic shifts of the two sites. Shown also are simulations using the parameters listed in Table 1. (a) More intense component; (b) less intense component.

Zwanziger, Youngman JNCS 168(1994)293-297

Boroxyl ring fraction ~ 75%

Table 1
Summary of the NMR parameters characterizing the two boron sites in borate glass, obtained by different procedures as described in the text. Shifts are relative to $Et_2O \cdot BF_3$

Parameter	Site 1	Site 2
$\delta_{iso}^{(CS)}$:	18.1 ± 1.2 ppm	13 ± 1 ppm
$(e^2qQ/h)\sqrt{1+\eta^2/3}$:	2.68 ± 0.09 MHz	2.56 ± 0.09 MHz
η:	0.2 ± 0.1	0.2 ± 0.1
Intensity:	$75 \pm 2\%$	$25 \pm 2\%$

Zwanziger, Youngman JNCS 168(1994)293-297

^{11}B in alkali thioborate glasses

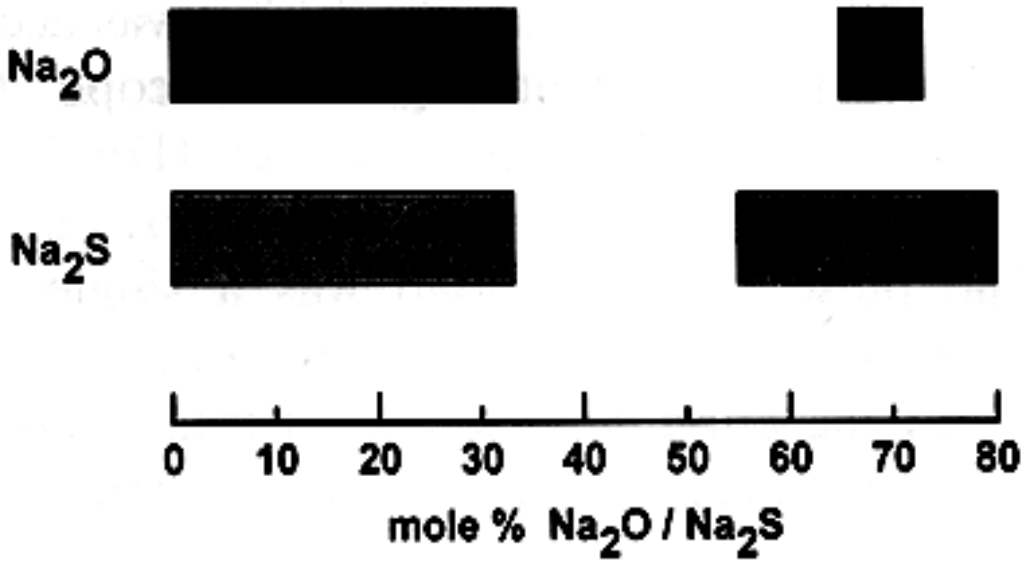

Fig. 3. Comparison of glass-forming regions in systems $Na_2X + B_2X_3$ (X = O, S) (oxide data from Ref. [32]).

Sills and Martin, JNCS, 168(1994)86-96

v-B_2O_3 compared to v-B_2S_3

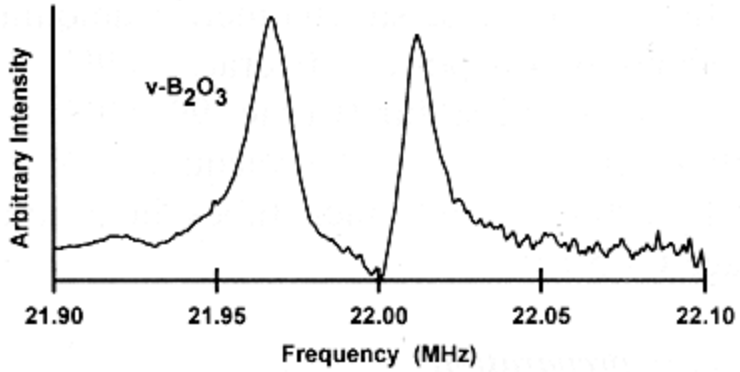

Fig. 5. ^{11}B NMR spectrum of vitreous B_2O_3.

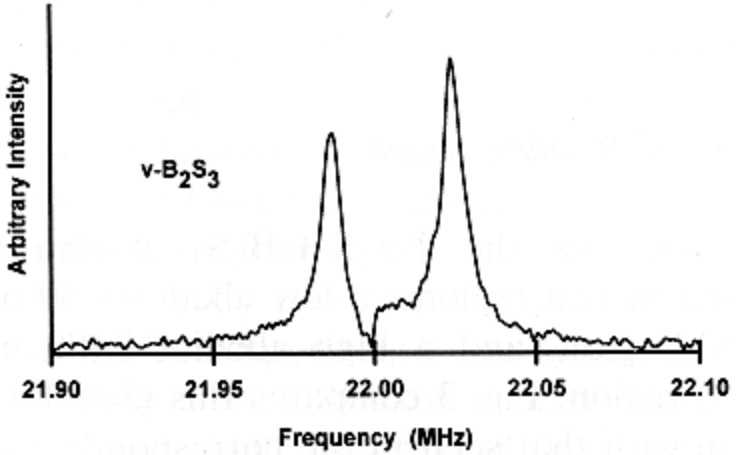

Fig. 4. ^{11}B NMR spectrum of vitreous B_2S_3.

Sills and Martin, JNCS, 168(1994)86-96

$Na_2S + B_2S_3$ glasses

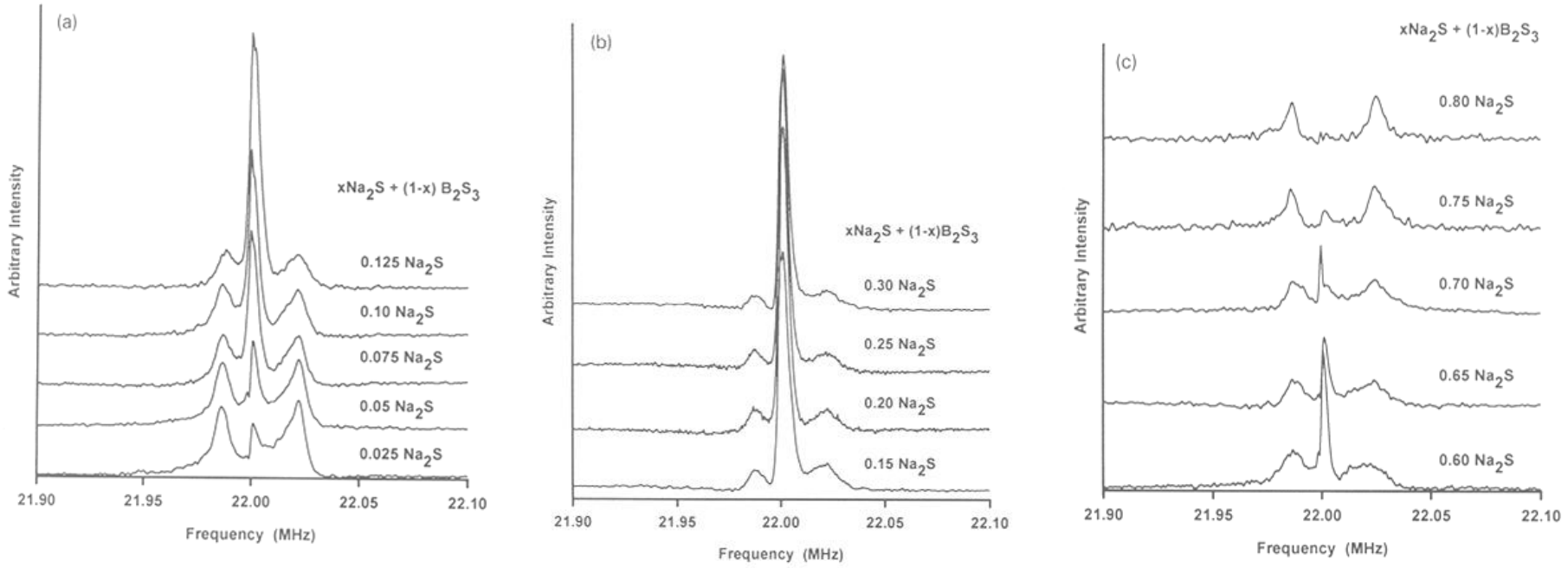

Fig. 6. (a) ^{11}B NMR spectra of low alkali $xNa_2S + (1-x)B_2S_3$ glasses, $0.025 \le x \le 0.125$. (b) ^{11}B NMR spectra of low alkali $xNa_2S + (1-x)B_2S_3$ glasses, $0.15 \le x \le 0.30$. (c) ^{11}B NMR spectra of high alkali $xNa_2S + (1-x)B_2S_3$ glasses, $0.60 \le x \le 0.80$.

Sills and Martin, JNCS, 168(1994)86-96

B4 in alkali thioborate glasses

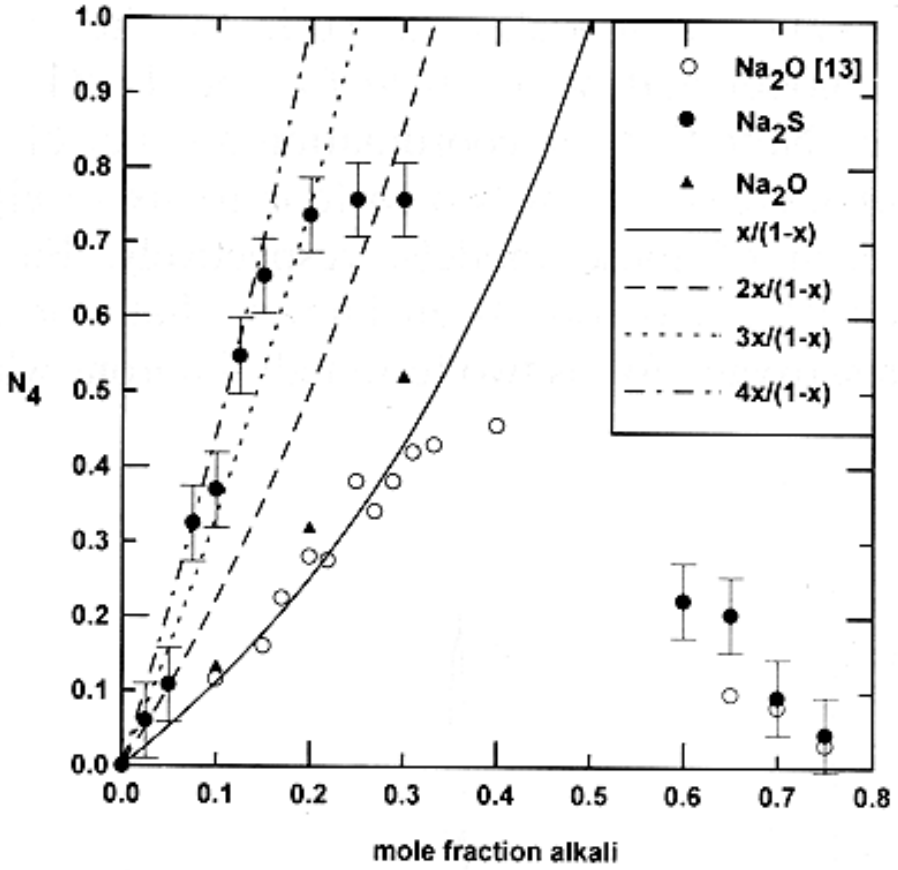

Fig. 8. N_4 versus mole fraction alkali for $Na_2S + B_2S_3$ glasses. Data for oxide glasses from Ref. [13] and from our own work are included for comparison.

Sills and Martin, JNCS, 168(1994)86-96

N4 in alkali thiobrate glasses

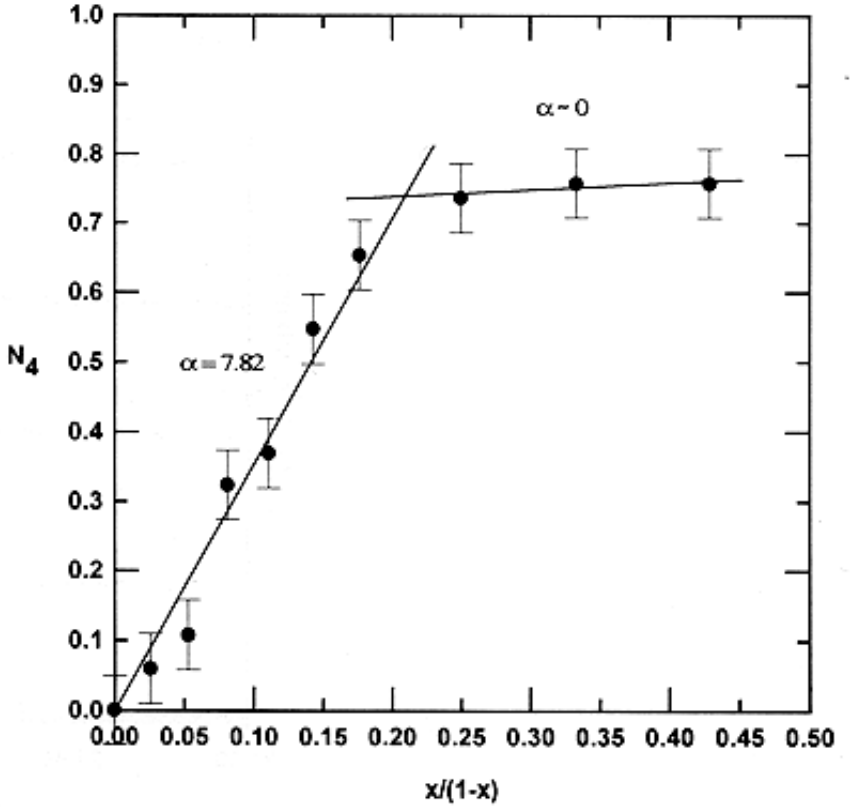

Fig. 9. N_4 versus $x/(1-x)$ for $Na_2S+B_2S_3$ glasses. Note two different slopes indicating two regions of different boron conversion rates.

Sills and Martin, JNCS, 168(1994)86-96

C-$Na_2B_4S_7$

N4 = 1, no quadrupole broadened line

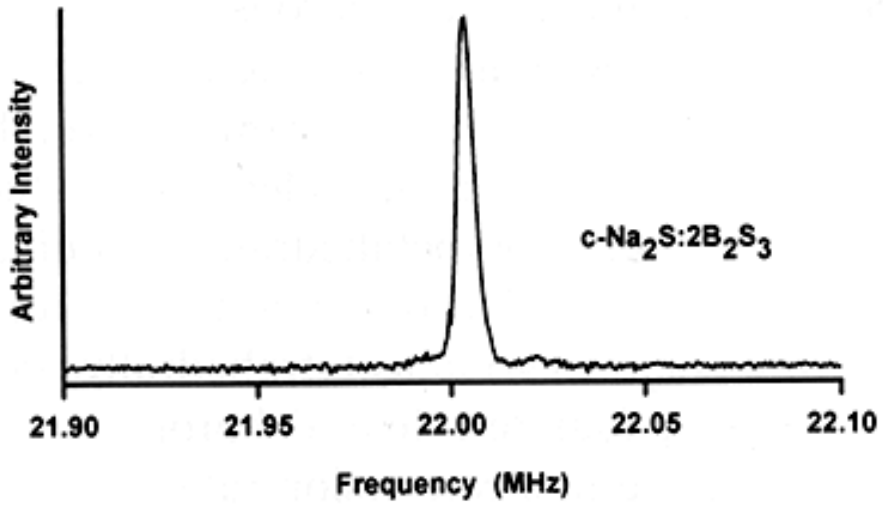

Fig. 11. ^{11}B NMR spectrum of crystalline sodium dithioborate, $Na_2S \cdot 2B_2S_3$.

Sills and Martin, JNCS, 168(1994)86-96

$xCs_2S + (1\text{-}x)B_2S_3$ ^{11}B NMR

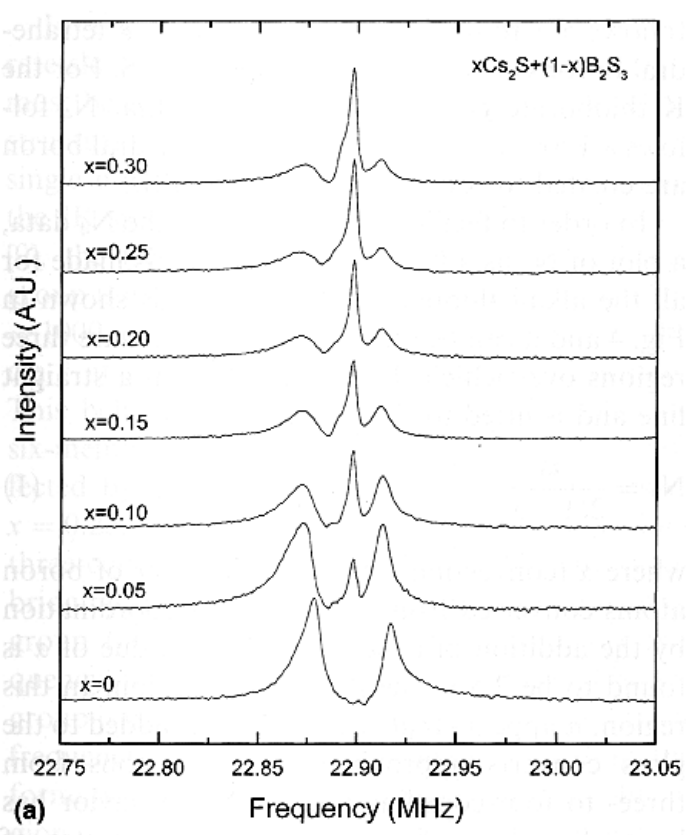

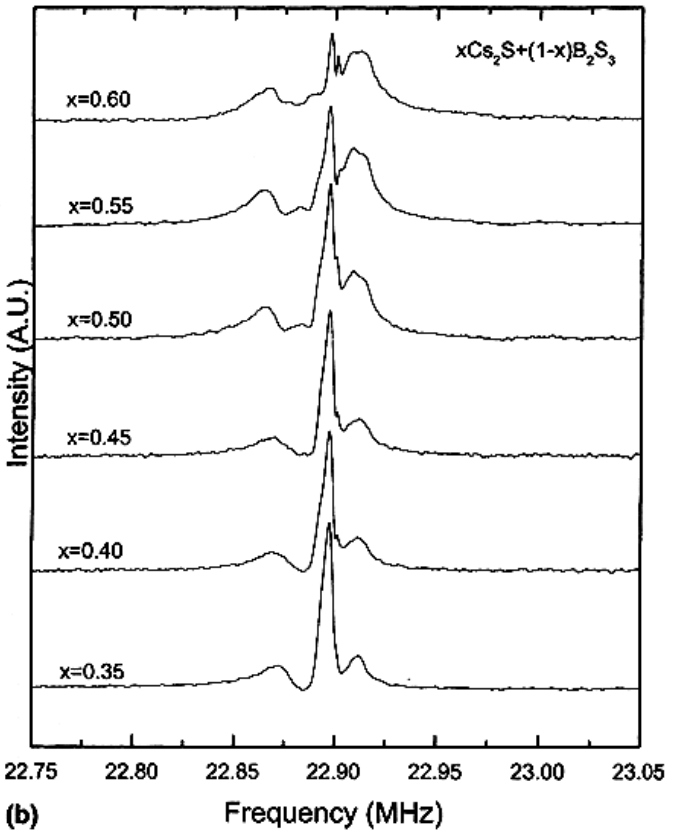

Fig. 2. ^{11}B NMR spectra of $xCs_2S + (1-x)B_2S_3$ glasses in the (a) $0 < x < 0.3$ region and (b) $0.35 < x < 0.6$ region.

Cho, Meyer, Martin JNCS 270(2000)205-214

N4 in x(Rb, Cs)$_2$S + (1-x)B_2S_3 Glasses

$Cs_2S + B_2S_3$

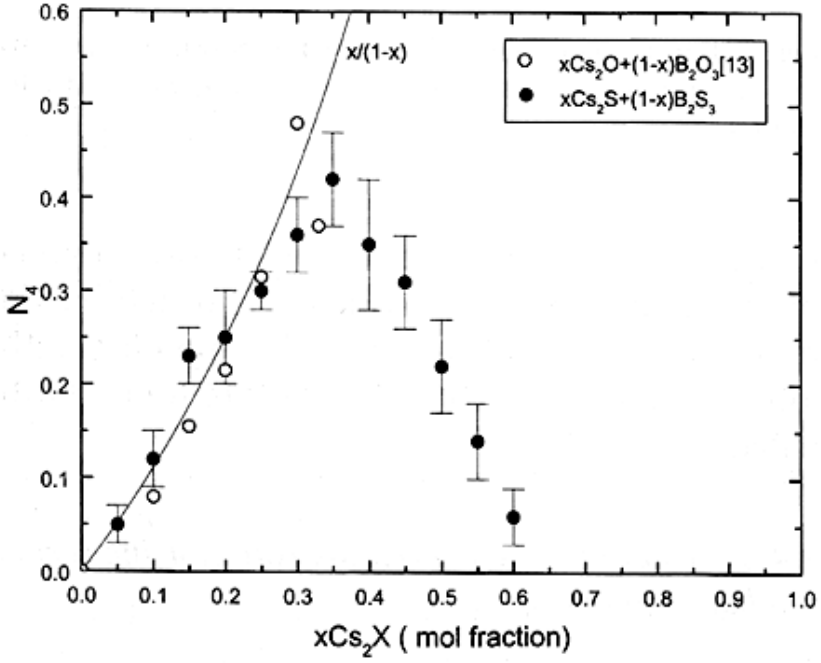

Fig. 7. N_4 vs mole fraction alkali for $Cs_2X + B_2X_3$ systems (X = O, S).

$Rb_2S + B_2S_3$

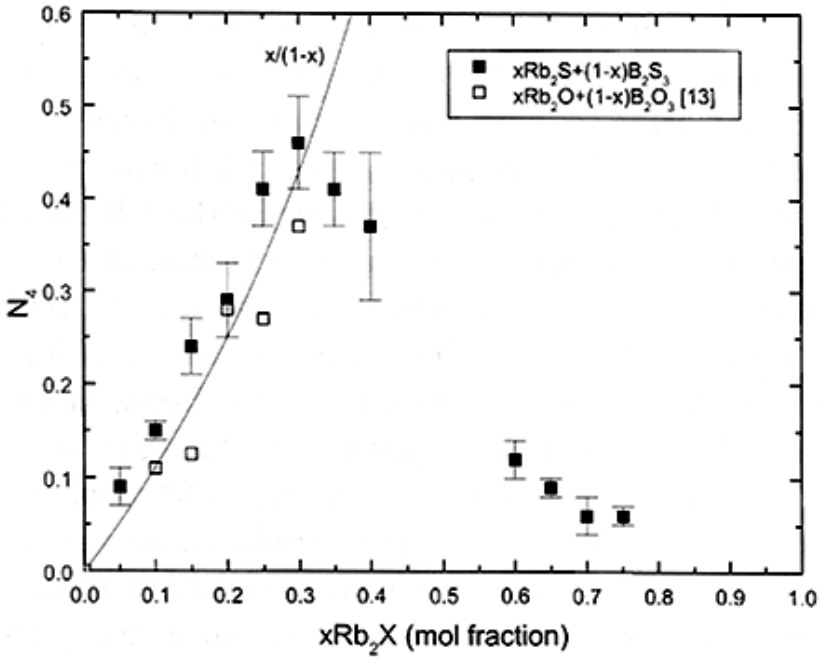

Fig. 3. N_4 vs mole fraction alkali for the $Rb_2X + B_2X_3$ systems, where X = O and S.

Cho, Meyer, Martin JNCS 270(2000)205-214

N4 in $xM_2S + (1-x)B_2S_3$ Glasses

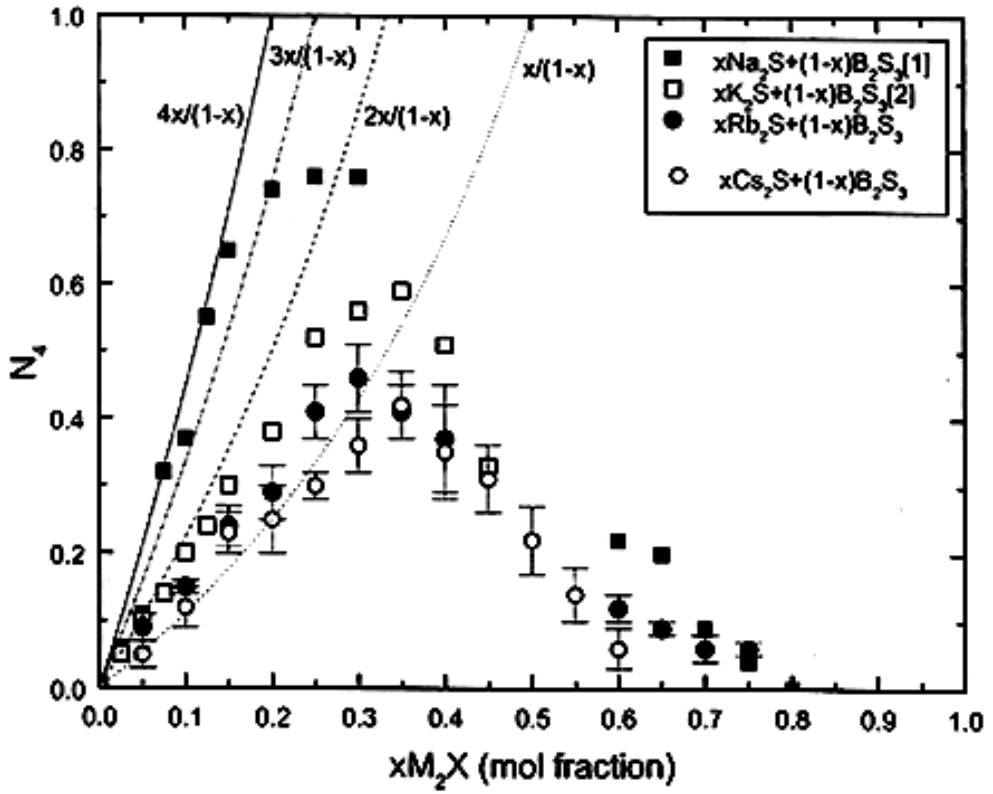

Fig. 8. N_4 vs. xM_2S (M = Na, K, Rb, and Cs; x = composition).

Cho, Meyer, Martin JNCS 270(2000)205-214

N4 in alkali thioborate glasses

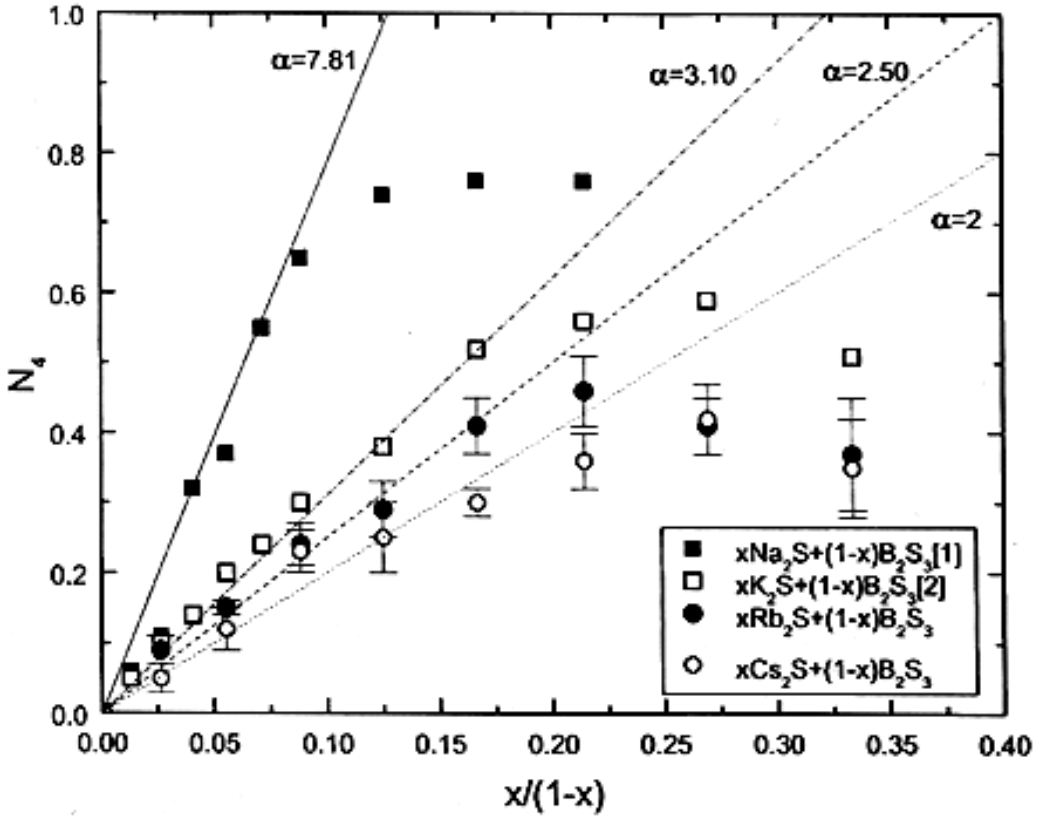

Fig. 4. N_4 vs $x/(1-x)$ for $M_2S+B_2S_3$ glasses, where M = Na, K, Rb and Cs.

Cho, Meyer, Martin JNCS 270(2000)205-214

Dithioborate group: $Cs_2B_4S_7$

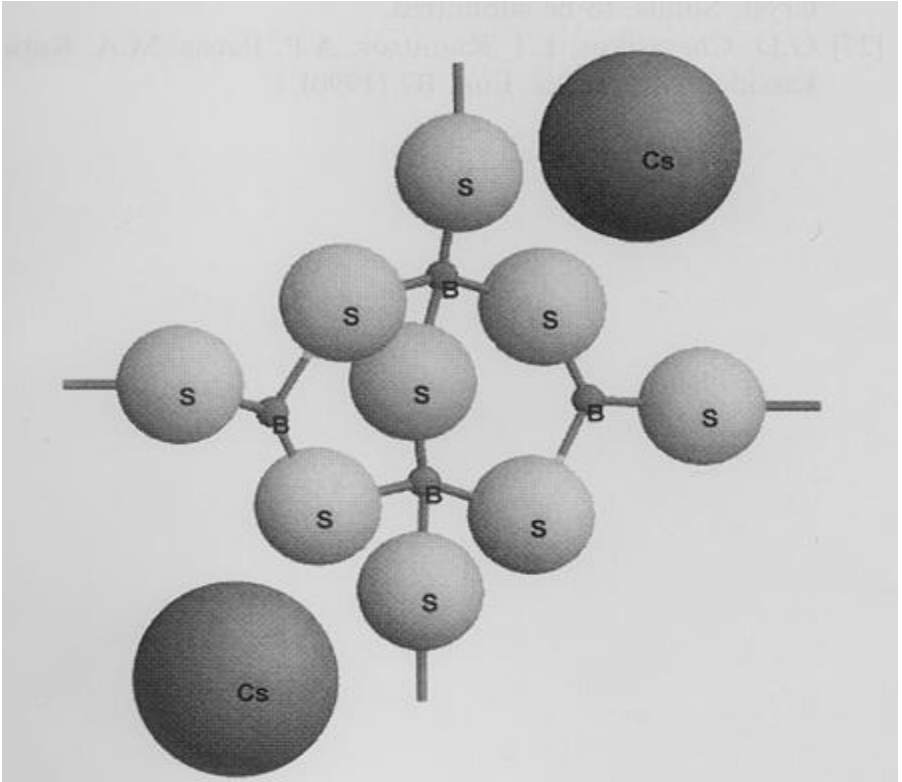

Fig. 9. Possible structures of cesium dithioborate polycrystalline phase.

Cho, Meyer, Martin JNCS 270(2000)205-214

Formation of "normal" B4 in $Cs_2S + B_2S_3$ glasses

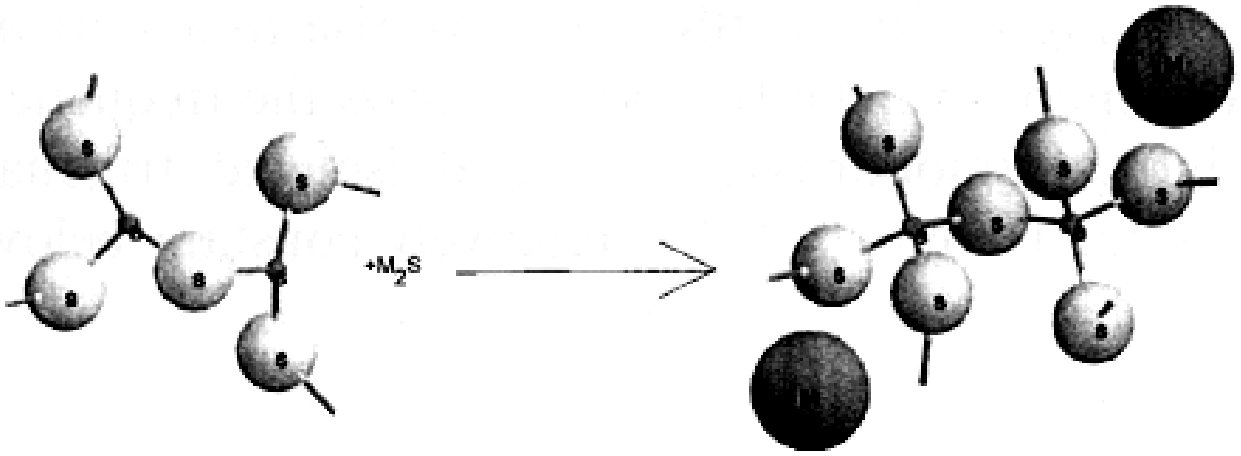

Fig. 6. Formation of 'normal' tetrahedral boron sites with the conversion rate of two for $M_2S + B_2S_3$ glasses, where M = Rb and Cs.

Cho, Meyer, Martin JNCS 270(2000)205-214

Dithioborate structure with N4 = 1

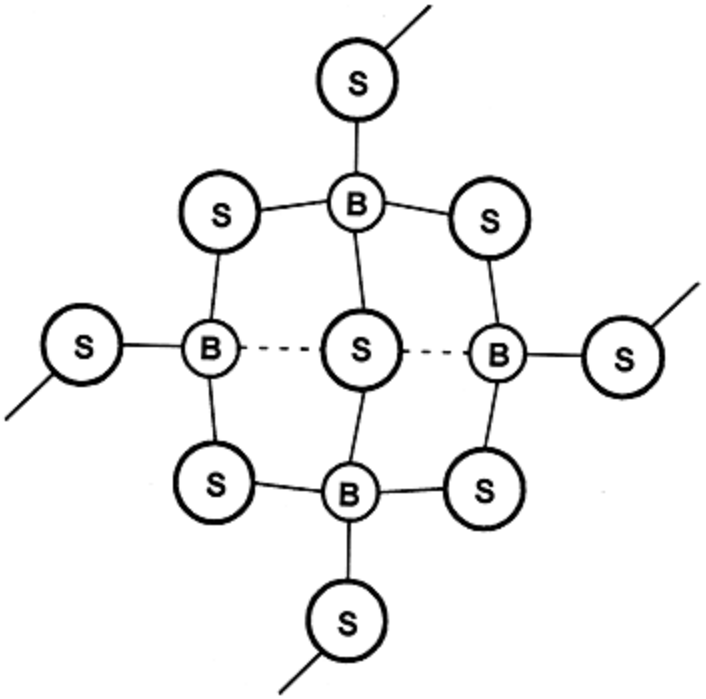

Fig. 12. Proposed structural unit containing tetrahedrally coordinated sulfur.

Sills and Martin, JNCS, 168(1994)86-96

$Na_6B_{10}S_{18}$ Crystal structure with N4 = 1

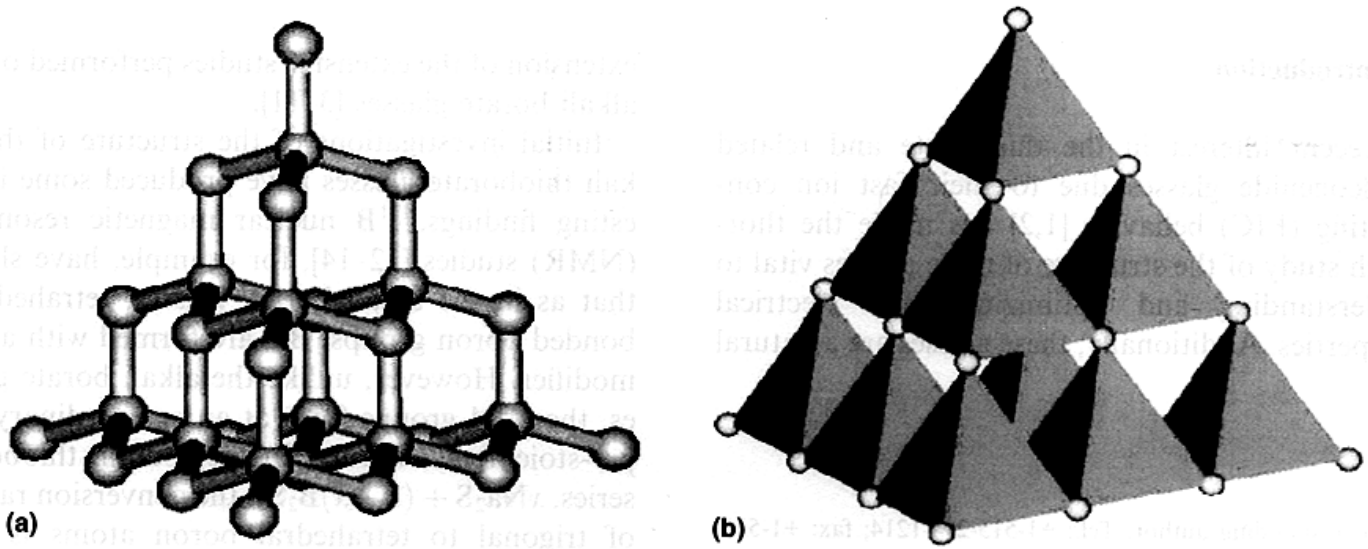

Fig. 1. Pyramidal structure of $B_{10}S_{18}^{6-}$ unit proposed by zum Hebel et al. [16]. (a) Shows the ball-and-stick model of the structure with sulfur atoms around the outer edges. (b) Shows the same structure with the boron tetrahedra shown as pyramids and highlights the fact that the trigonally coordinated sulfur atoms are located at the center of each of the four faces.

Royle, Cho, Martin JNCS 279(2001)97-109

Spin-Lattice relaxation time measurements

- When the spins are flipped, it takes time for the spins to relax to the lower (ground) energy state
- This time is characterized by the spin-lattice relaxation time, T1
- T1 is typically very long for solids
  - Few mechanisms to enable the spin to release its spin energy
- T1 is typically very short for liquids
  - Rapid atomic, ionic, and/or molecular motion helps release spin energy through diffusion

Spin-Lattice relaxation time measurements

- Spin lattice relaxation T1 can be used therefore to examine diffusion processes
  - Temperature dependence of T1 can be used as a measure of molecular or atomic diffusion
  - Temperature dependence of T1 can also be used as a measure of ionic diffusion
- Temperature dependence of T1 is a measure of atomic level displacements, diffusion
- T1 can be compared to ionic conduction processes in glasses
  - Nuclear Spin Lattice Relaxation Time, T1
  - Nuclear Spin Lattice Relaxation Time, 1/T1≡ R1

Determination of the DAEs in Glass

- Direct measurement through NMR NSLR data
- Conduction process is by the percolation through low barrier sites
- Conductivity will only measure the low energy barriers
- NSLR measures all cations, both contribute to NSLR T_1

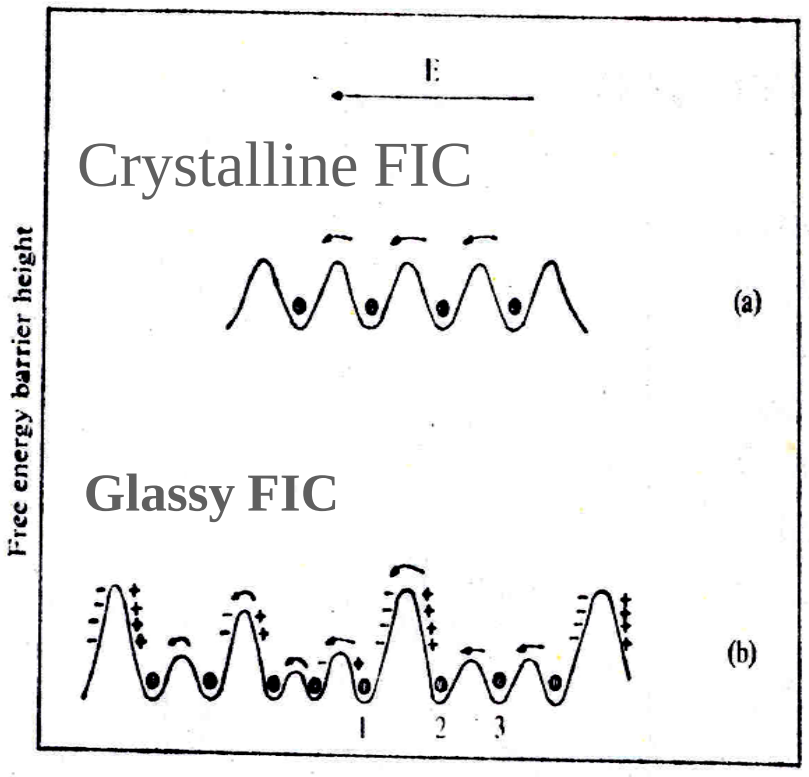

Stevels & Taylor DAEs model,

NSLR to DAE to Conductivity

NSLR → DAE → Conductivity

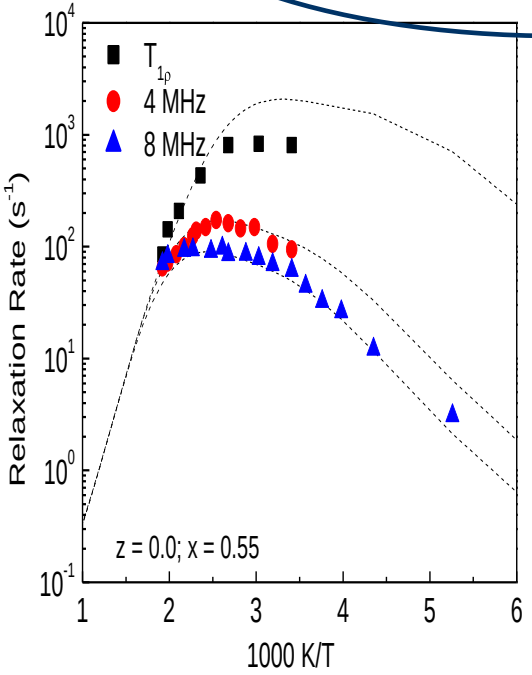

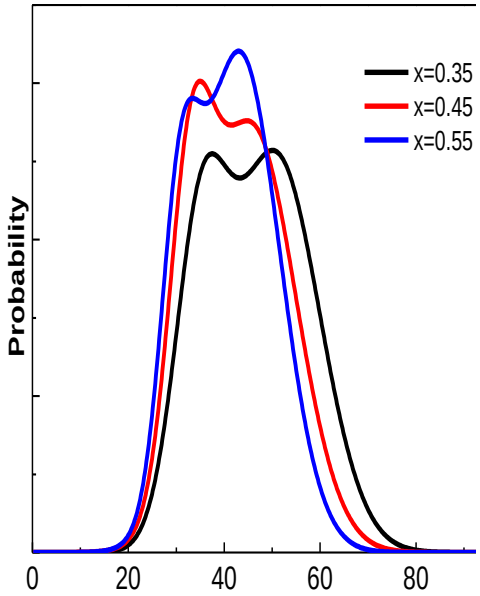

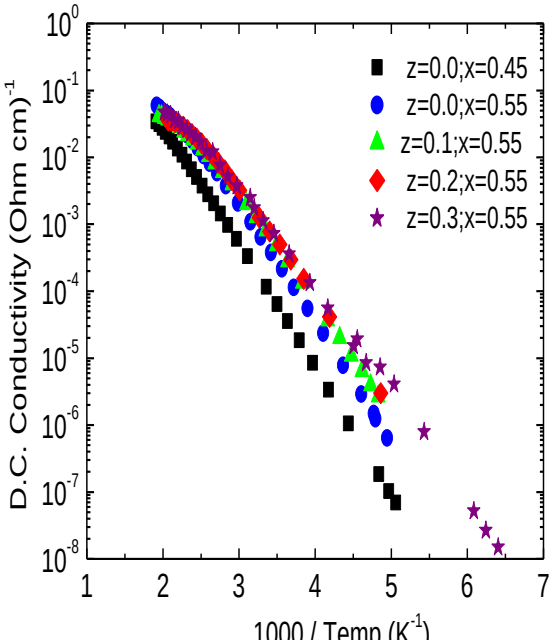

NMR Relaxation of Spin Energy

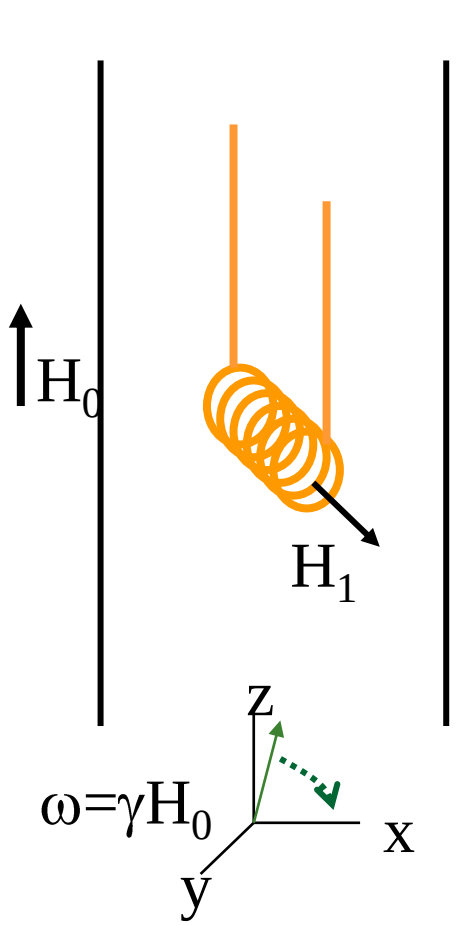

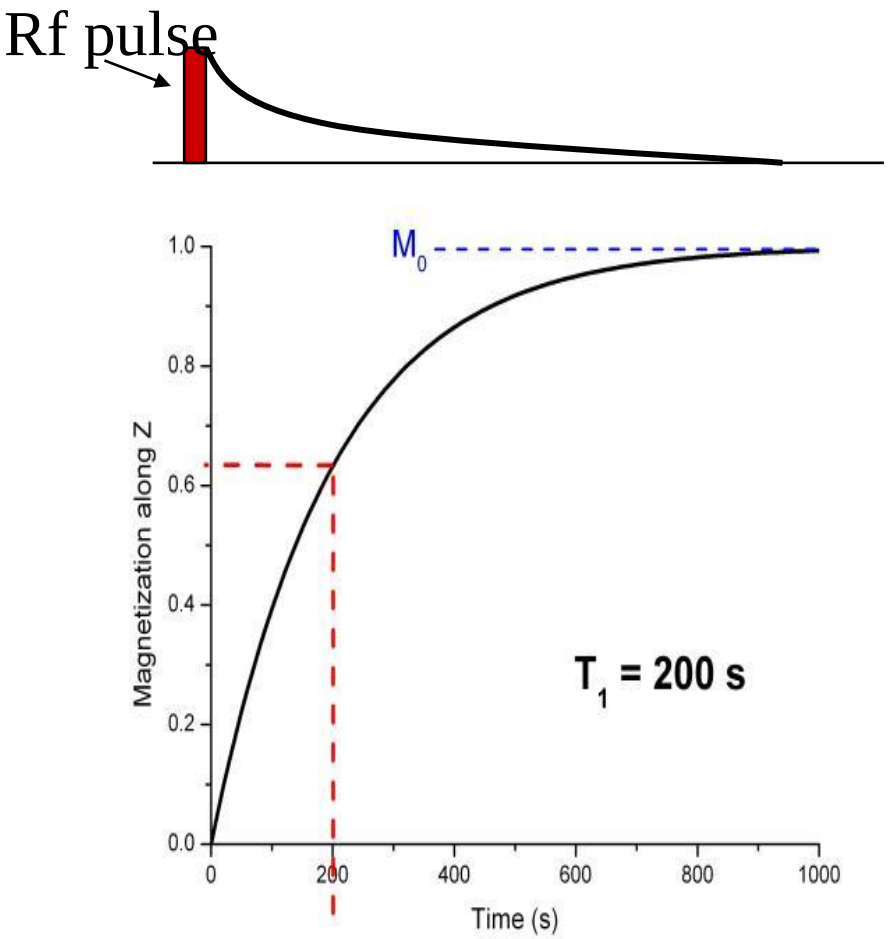

Fluctuations from Ionic Motion

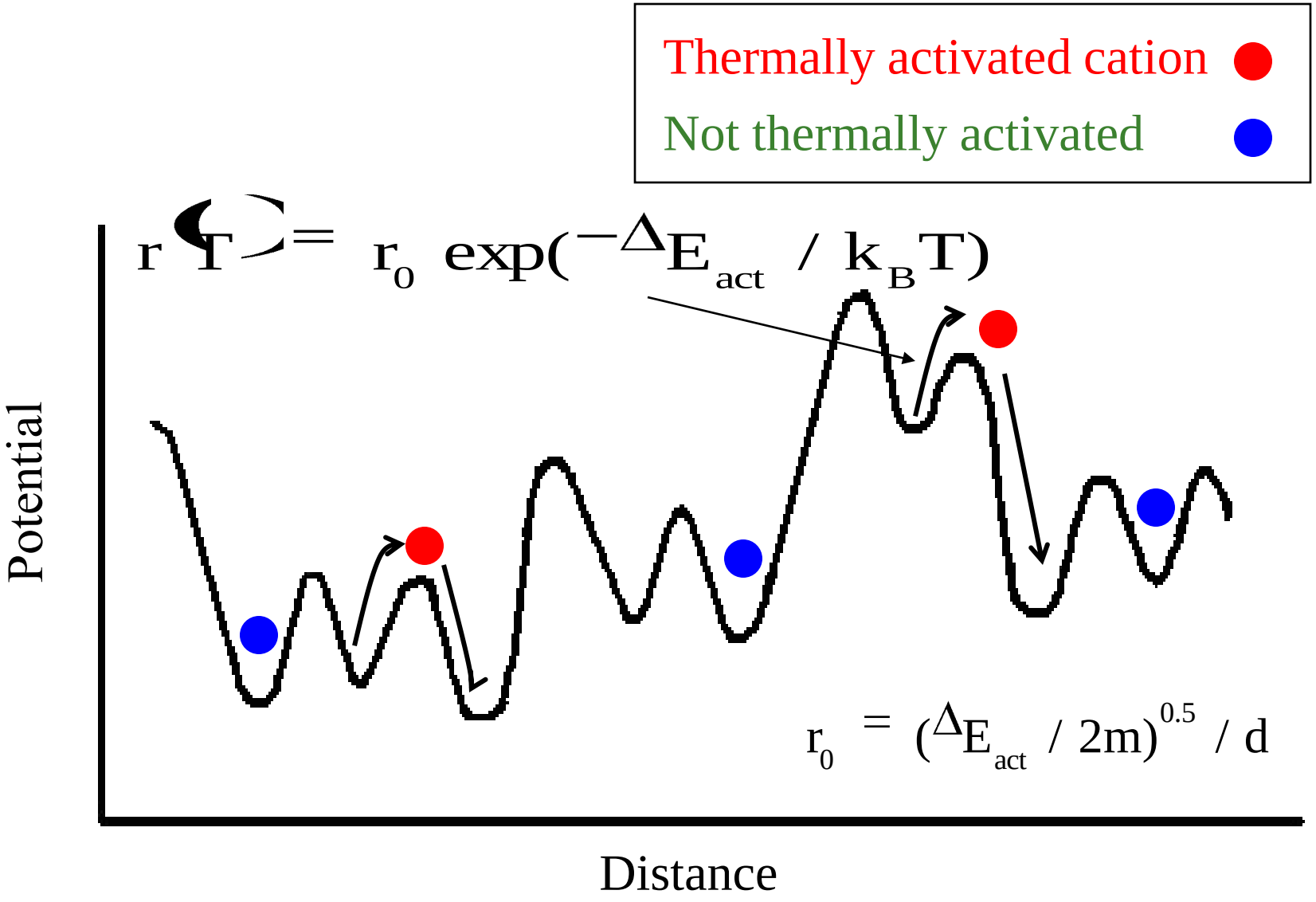

Bloombergen-Purcell-Pound (BPP) Theory

$$R_1(T) = \frac{1}{T_1(T)} = C_1\left[\frac{\tau_c(T)}{1+\omega_L^2\tau_c(T)^2} + \frac{4\tau_c(T)}{1+4\omega_L^2\tau_c(T)^2}\right]$$

$$\tau_c(T) = \frac{1}{r(T)}$$

Single relaxation time theory

R_1 = relaxation rate

T_1 = relaxation time

ω_L = Larmor frequency

C_1 = coupling constant

τ_c = correlation time

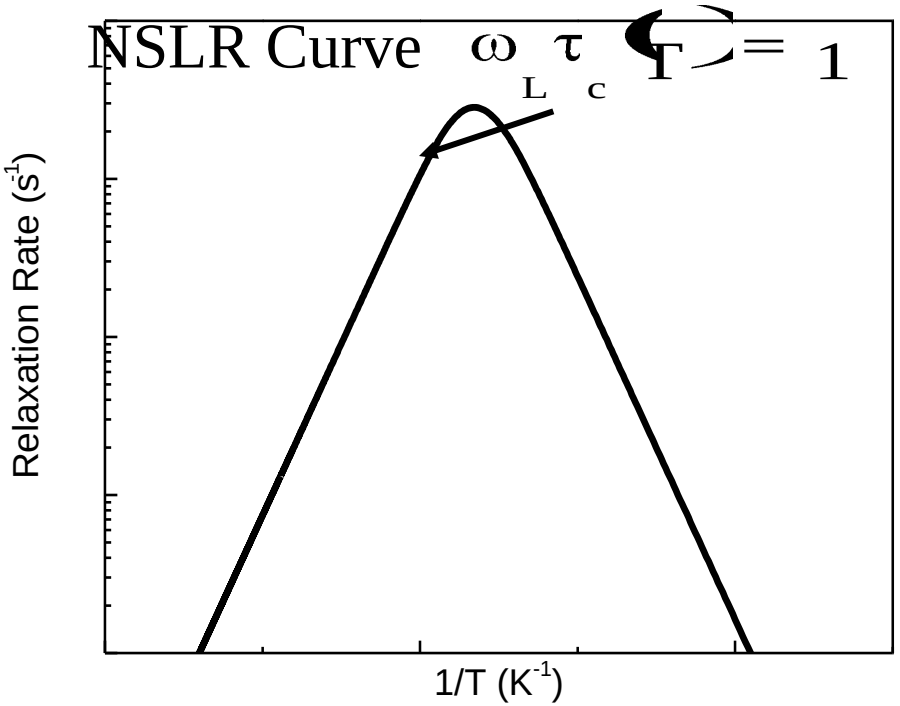

Low Temperature Asymmetry

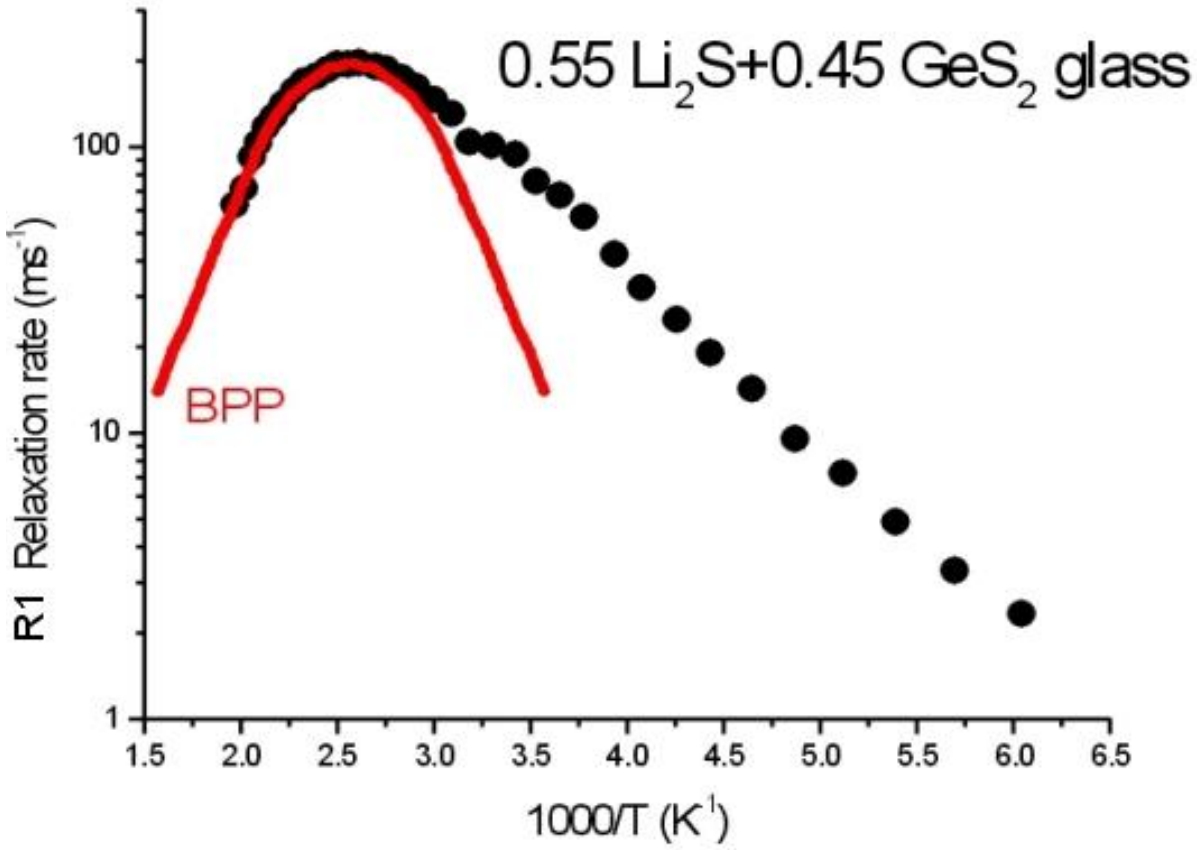

K. H. Kim, Solid State Ionics 91 (1996).

Distribution of Activation Energies

$$Z_{NMR}(\Delta E_a) = \frac{1}{\sqrt{2\pi}\Delta E_b^2} \exp\left[-\frac{(\Delta E_m - \Delta E_a)^2}{2\Delta E_b^2}\right]$$

ΔE_m = average

ΔE_b=standard deviation

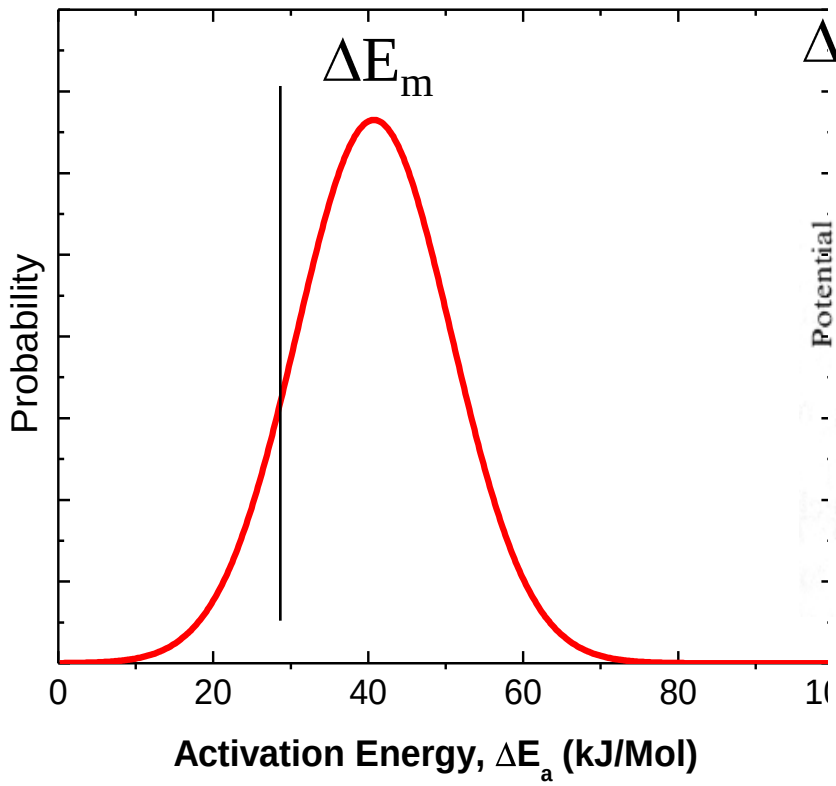

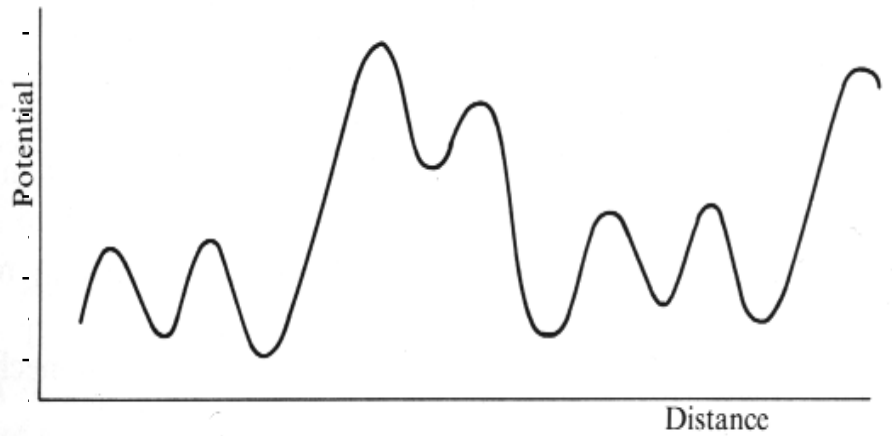

J. Zarzycki, Glasses and the Vitreous State (1991).

NMR NSLR Data

- Determination of the DAEs from NSLR T_1 measurements

$$1/T_1(\omega_L, T) \equiv R_1(\omega_L, T) = C \int_0^\infty \frac{\tau_a}{1+\omega_L^2 \tau_a^2} + 4\frac{\tau_a}{1+4\omega_L^2 \tau_a^2} Z_{NMR}\, dE_{NMR}$$

$$Z_{NMR}(E_a) = (1-y)\frac{1}{\sqrt{2\pi}E_b^2}\exp\left[-\frac{(E_m - E_a)^2}{2E_b^2}\right] + y\frac{1}{\pi}\left[\frac{E_1}{E_1^2 + (E_m - E_a)^2}\right]$$

- Gaussian DAEs with Lorentzian "tail", y ~ 0.2, to account for low temperature, high frequency "extra" relaxation

DAEs from FIC $Li_2S + GeS_2$ Glasses

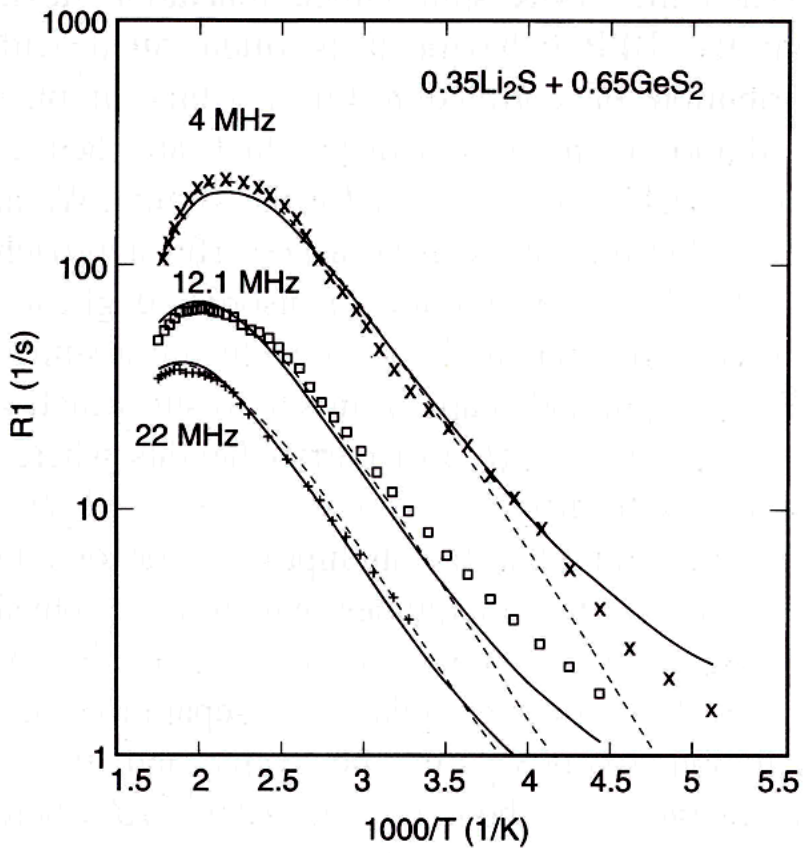

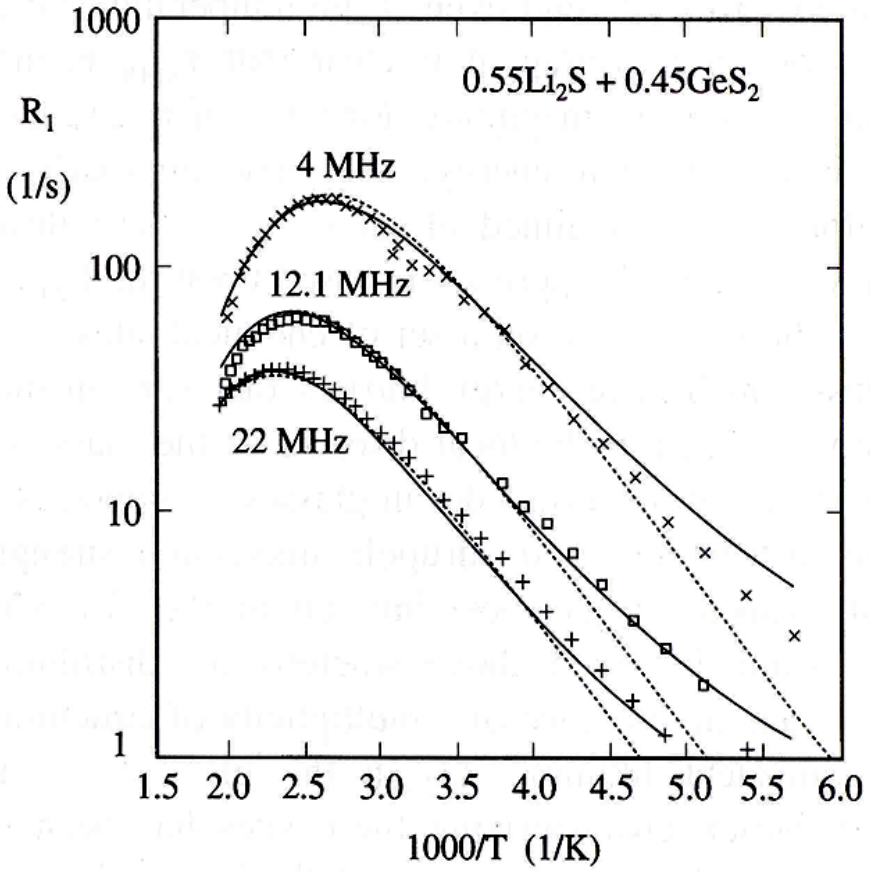

DAEs from FIC $Li_2S + GeS_2$ Glasses

- Average of distribution shifts to smaller activation energies with increasing Li_2S
- Distribution does not change shape significantly, all have ~ same FWHM
  - 0.55 Glass is slightly narrower

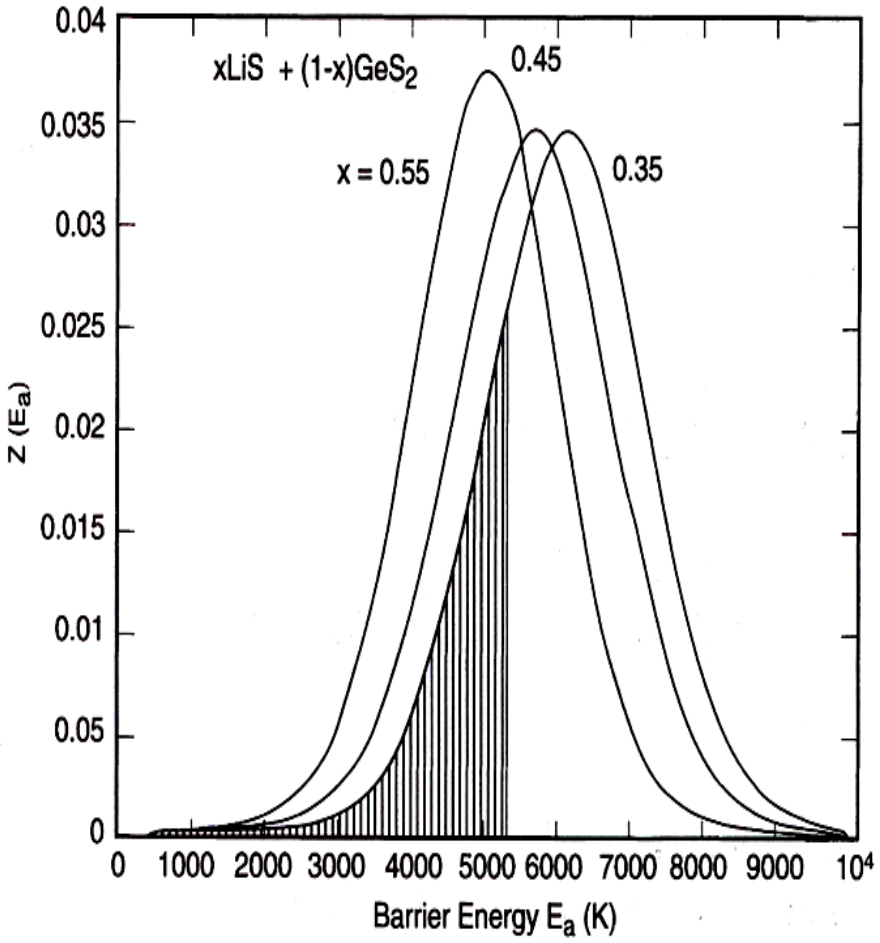

Multiple FIC Dynamics in Glass

- "Multiple Channel" ion relaxation in FIC glasses
- R_1 data show evidence of multiple relaxation processes
- Fast process at low T, slower process at higher T
- Alkali thioborate glasses are speciated into tetrahedral borons and trigonal borons with NBS
- Are "slow" Li^+ ions associated with NBS?
- Are "faster" Li^+ ions associate with $BS_{4/2}^-$ groups?

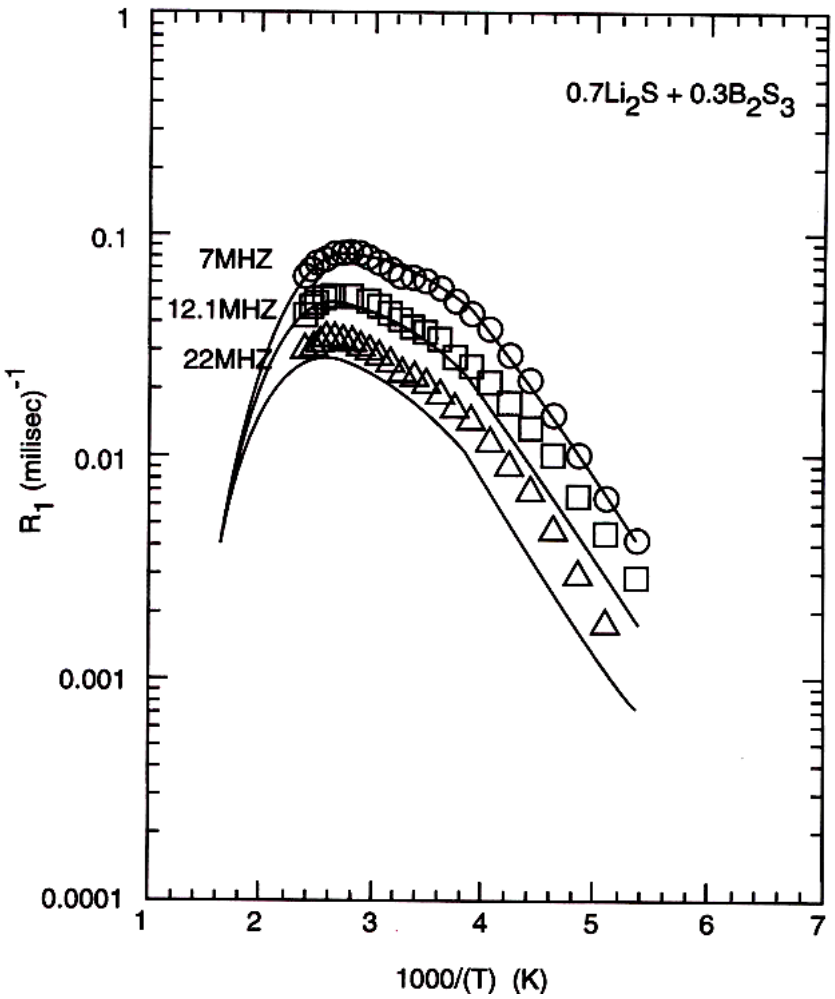

Multiple FIC Dynamics in Glass

- Relaxation spectra of both mobile Li^+ ions and immobile frame work B ions were measured
- Multiple-channel relaxation was observed for Li^+ ions
- BS_3 and BS_4 units have different relaxation rates and hence difference DAEs to characterize their dynamics
- N_4 of $0.7Li_2S$ is 0.05
- Most Li^+ ions are associated with BS_3^{3-} groups, as evidenced in the DAEs

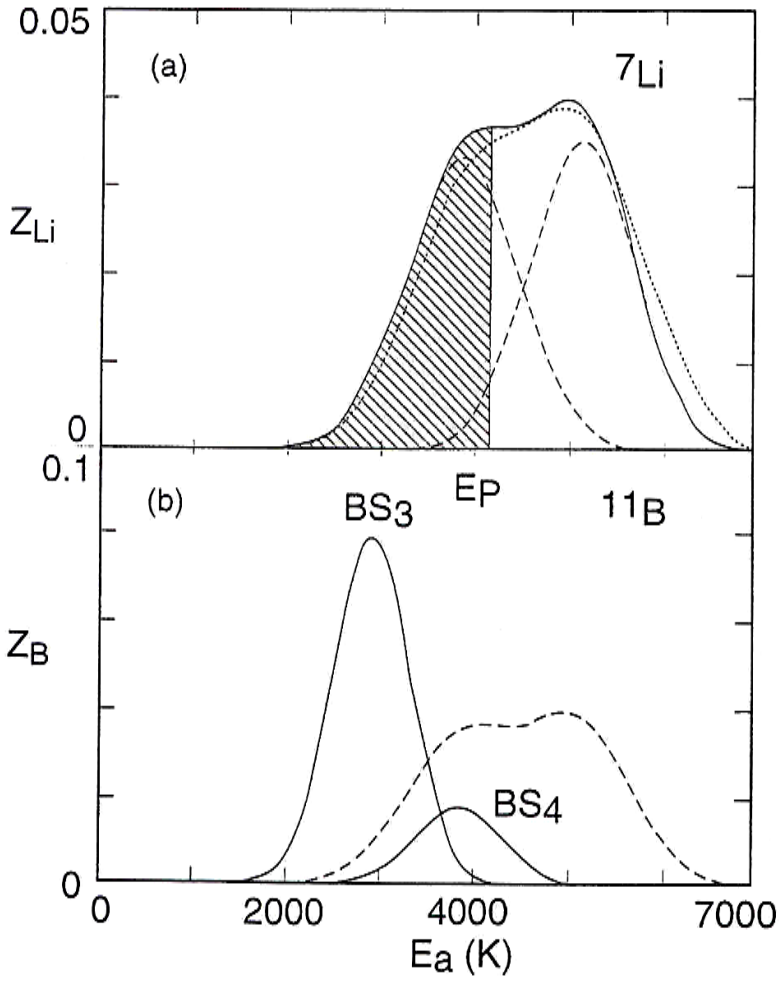

Two Distributions

$xLi_2S + (1-x)[0.5B_2S_3 + 0.5GeS_4]$

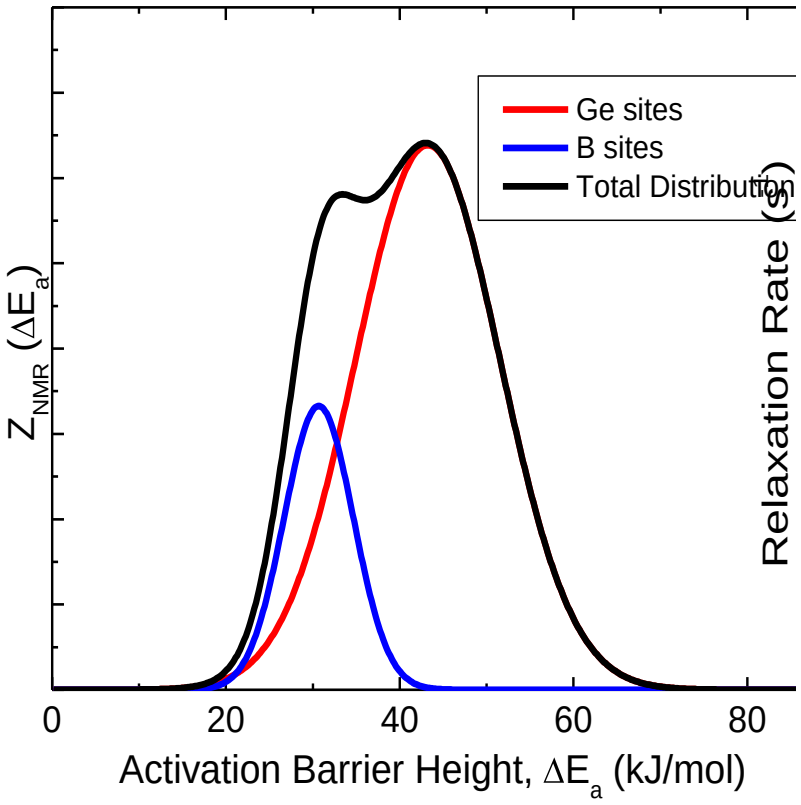

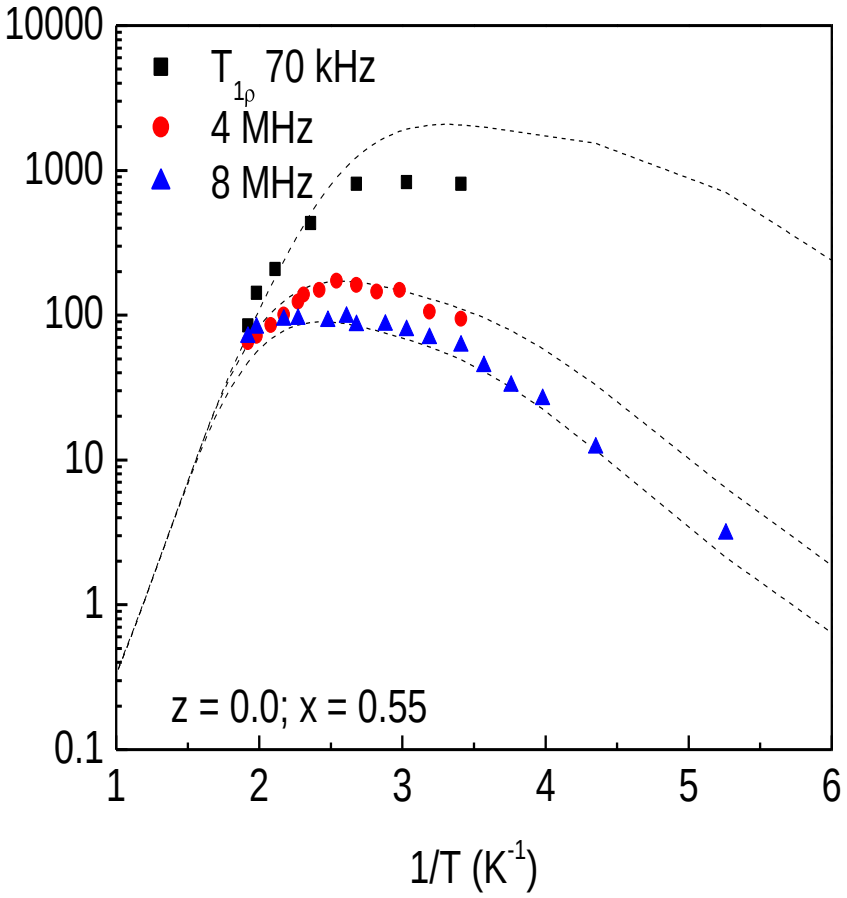

Effects of Li_2S Addition

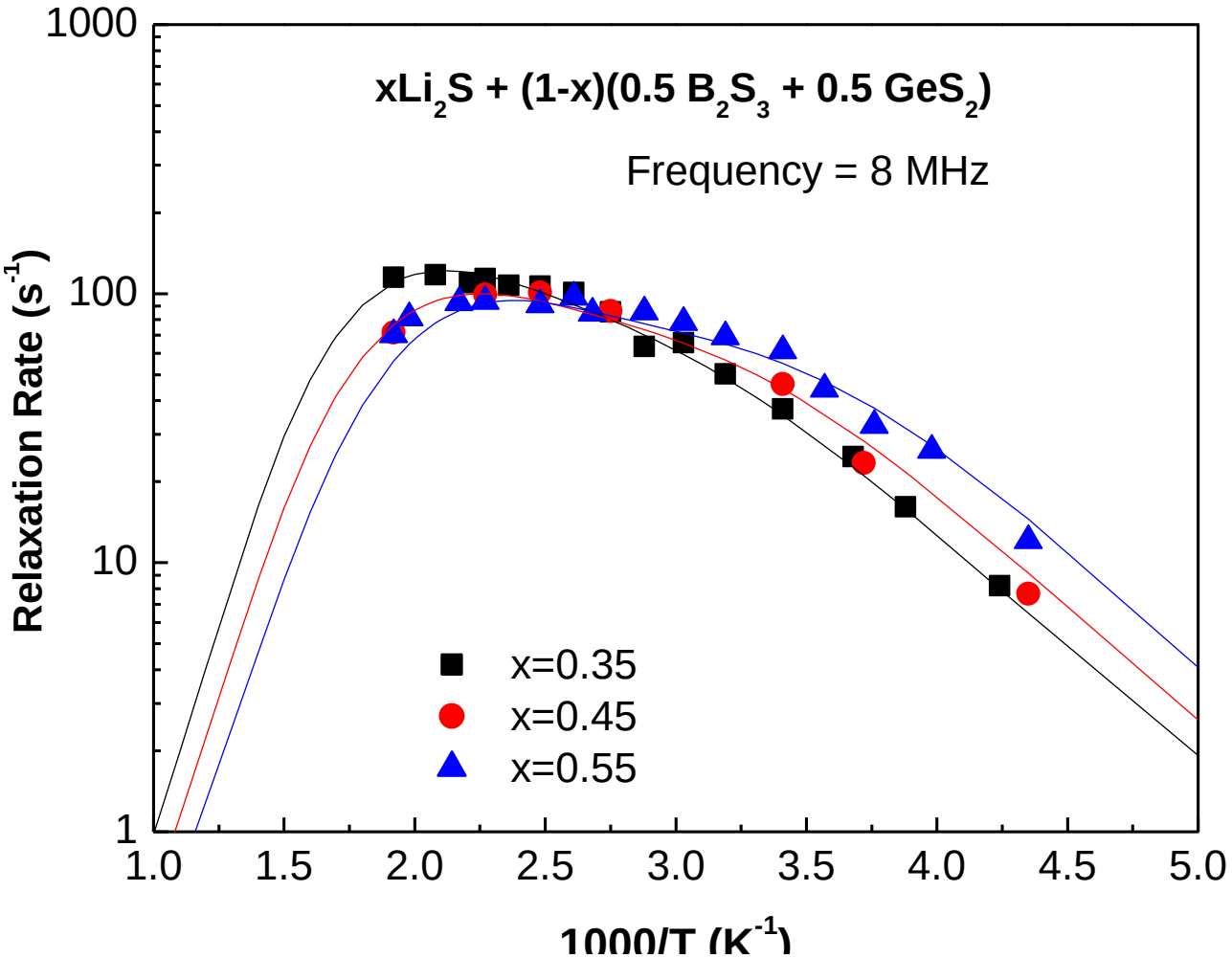

Average Activation Energy

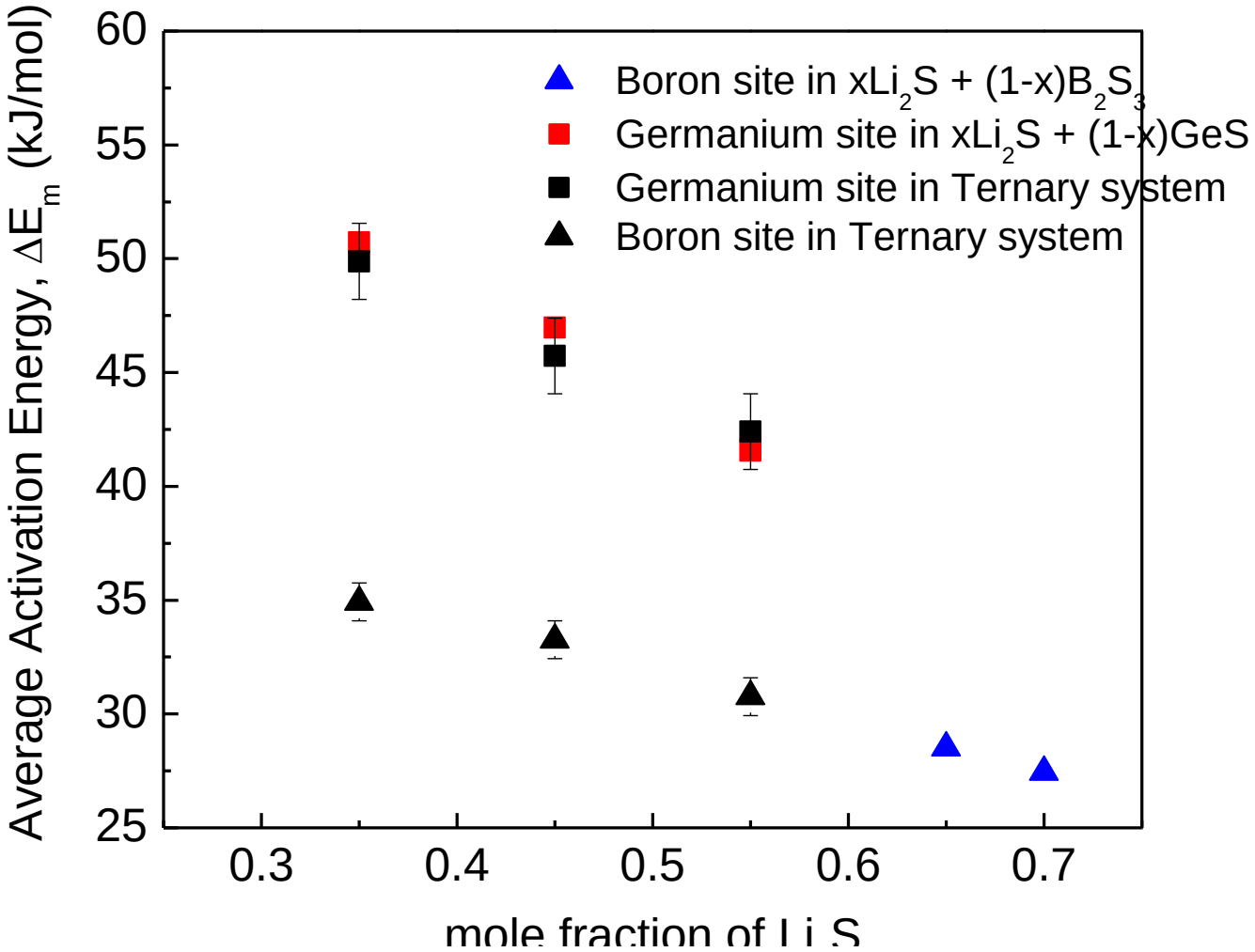

LiI doped – Activation Energy

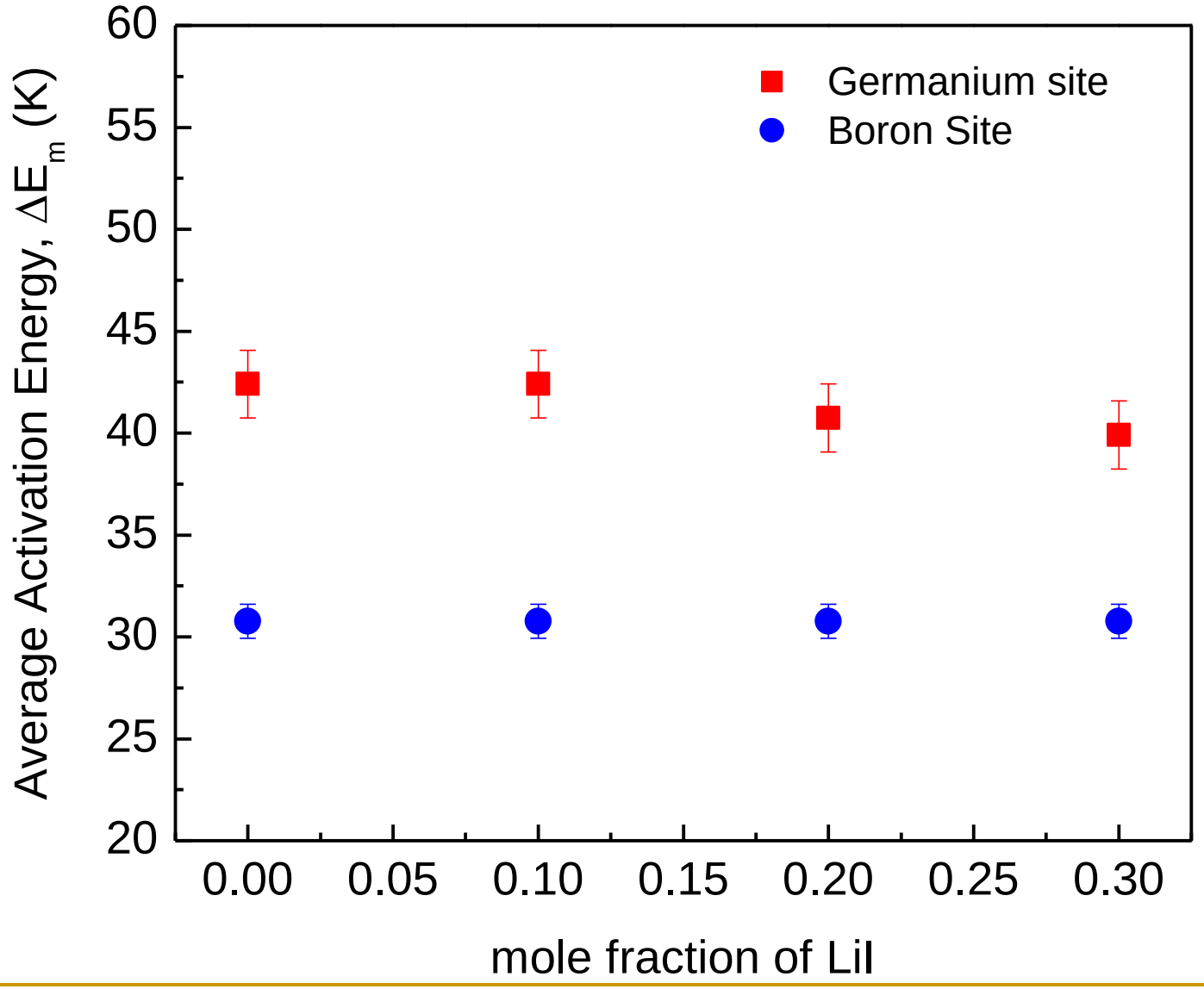

LiI Addition

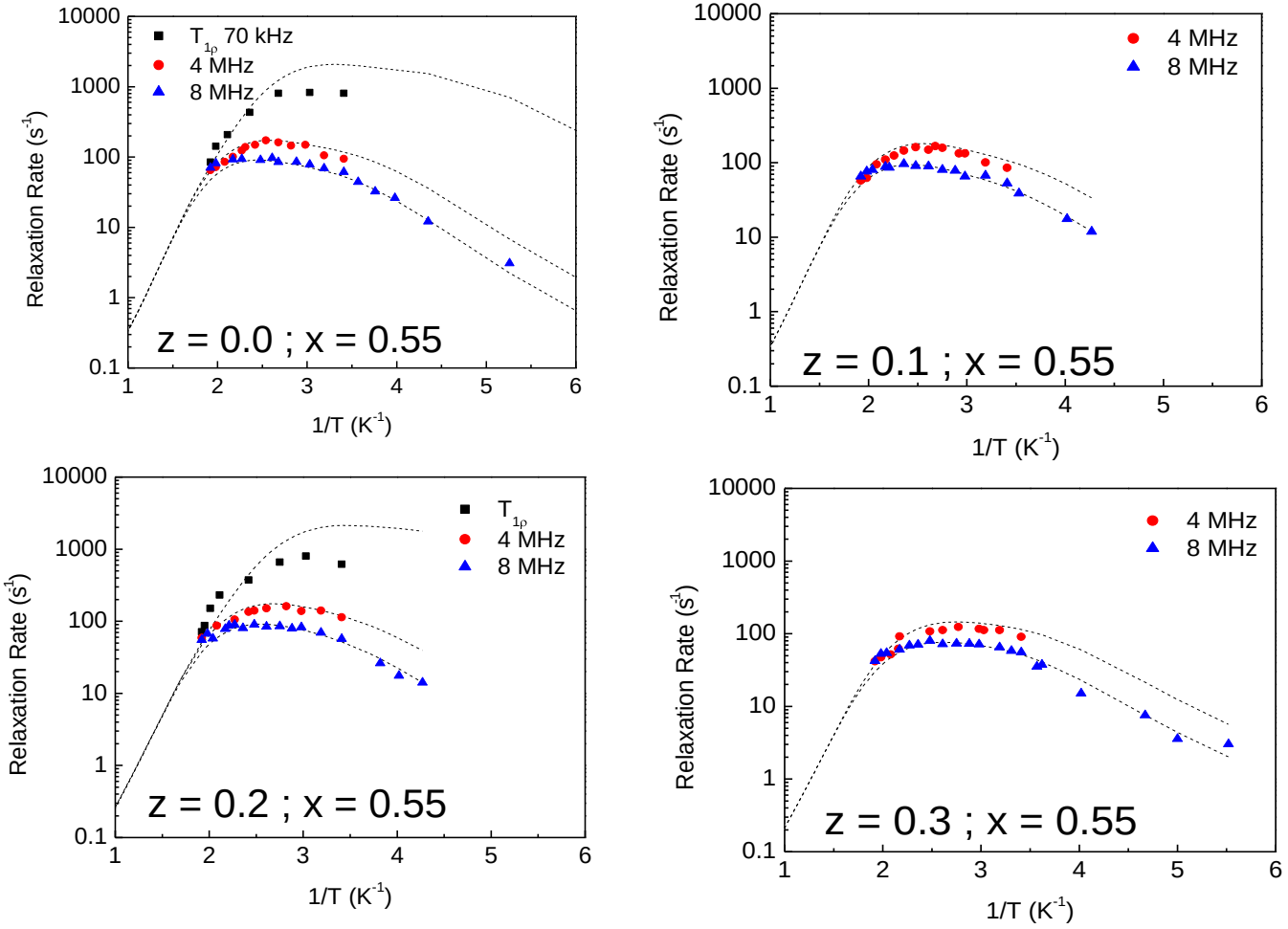

Distribution of Activation Energies

$$xLi_2S + (1-x)(0.5\ B_2S_3 + 0.5\ GeS_2)$$

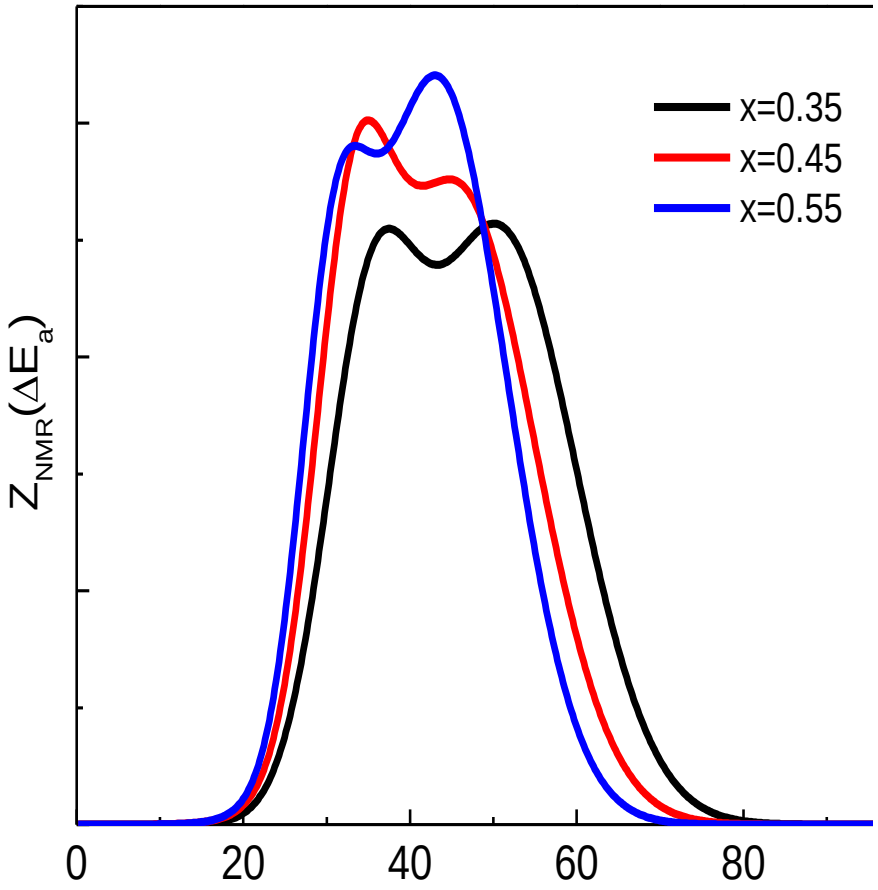

Distribution of Lithium atoms

Using coupling constants within 10% of binary values yielded approximate Lithium sharing fractions of:

Sample	Germanium sites	Boron sites
x=0.35	0.70	0.30
x=0.45	0.75	0.25
x=0.55	0.80	0.20

DAEs Treatment

- Using a DAEs to treat ion conduction in glass is not new
- Von Schweidler used a DRTs as early as 1907
  - *Ann. Physik.* ***24****(1907)711.*
- Cole and Cole, Cole and Davidson reported log Guassian DAEs
  - *J. Chem. Phys.* ***9****(1941) 341*
- H. E. Taylor used a DAEs to describe the dielectric relaxation
  - Modeling ε' and ε'' in soda-lime-silicate glass in 1955
  - *Trans. Fara. Soc.* ***51****(1955)873.*
- C. T. Moynihan used a log Guassian treatment
  - Modeling conductivity relaxation in CKN melts and glasses in 1972
  - *Phys. Chem. Glasses* ***13****(1972)171*